Modelling and controlling of polymer electrolyte fuel cell systems

Qi, Yuanxin

2021

Document Version:
Publisher's PDF, also known as Version of record

Modelling and Controlling of Polymer Electrolyte Fuel Cell Systems

YUANXIN QI
FACULTY OF ENGINEERING | LUND UNIVERSITY

Printed by Media-Tryck, Lund 2021 NORDIC SWAN ECOLABEL 3041 0903

Faculty of Engineering
Lund University
ISBN 978-91-7895-938-9
ISSN 0282-1990
ISRN LUTMDN/TMHP-19/1166-SE

Modelling and Controlling of Polymer Electrolyte Fuel Cell Systems

Modelling and Controlling of Polymer Electrolyte Fuel Cell Systems

by Yuanxin Qi

LUND
UNIVERSITY

Thesis for the degree of Doctor of Philosophy in Engineering
Thesis advisors: Docent. Martin Andersson
Faculty opponent: Prof. Kristian Etienne Einarsrud

To be presented, with the permission of the Faculty of Engineering of Lund University, for public criticism in the lecture hall KC:C, at the Division of Heat Transfer, Department of Energy Sciences on the 29th of October 2021 at 10:00.

Organization
LUND UNIVERSITY
Division of Heat Transfer
Department of Energy Sciences
Box 118
SE-221 00 LUND, Sweden

Document name
DOCTORAL DISSERTATION

Date of disputation
2021-10-29

Sponsoring organization

Author(s)
Yuanxin Qi

Title and subtitle
Modelling and controlling of polymer electrolyte fuel cell systems

Abstract
This thesis focuses on the modelling and controlling of polymer electrolyte fuel cell (PEFC) systems. A system level dynamic PEFC model has been developed to test the system performance (output voltage, reactants gas partial pressures, and stack temperature) for different operating conditions. The simulation results are in good agreement with the experimental data, which indicates that the PEFC model is well qualified to capture the dynamic performance of the PEFC system. Controlling strategies play a significant role in improving the fuel cell system's reliability. Novel model predictive control (MPC) controllers and proportional–integral–derivative (PID) controllers are proposed and implemented in different PEFC systems to control voltage and regulate temperature to enhance system performance. MPC controllers show superior performance to PID controllers in tracking the reference value, with less overshoot and faster response. A novel hydrogen selective membrane reactor (MR) is designed for methanol steam reforming (MSR) to produce fuel cell grade hydrogen for PEFC stack use. The backpropagation (BP) neural network algorithm is applied to find the mapping relation between the MR's operating parameters and the PEFC system's output performance. Simulation results show that the BP neural network algorithm can well predict the system behaviour and that the developed mapping relation model can be used for practical operation guidance and future control applications.

Key words
system level modelling, polymer electrolyte fuel cell systems, model predictive control, methanol steam reforming, membrane reactor, backpropagation neural network algorithm

Classification system and/or index terms (if any)

Supplementary bibliographical information

Language
English

ISSN and key title
0282-1990

ISBN
978-91-7895-938-9(print)
978-91-7895-937-2(pdf)

Recipient's notes

Number of pages
68

Price

Security classification

Modelling and Controlling of Polymer Electrolyte Fuel Cell Systems

by Yuanxin Qi

LUND
UNIVERSITY

Funding information: The thesis work was financially supported by the Chinese Scholarship Council and ÅForsk, 17-331.

Cover illustration: Lund University standard picture

Division of Heat Transfer
Department of Energy Sciences
Faculty of Engineering
Lund University
Box 118
SE–221 00 LUND
Sweden

ISBN: 978-91-7895-938-9 (print)
ISBN: 978-91-7895-937-2 (pdf)
ISSN: 0282-1990
ISRN: LUTMDN/TMHP-19/1166-SE

Printed in Sweden by Media-Tryck, Lund University, Lund 2021

"if you want something badly, just stand up and fight for it"
–"Reader"

Contents

List of publications

This thesis is based on the following publications, referred to by their Roman numerals:

I **Temperature control strategy for polymer electrolyte fuel cells**

Y.X. Qi, X.F. Li, S.A. Li, T.S. Li, M. Espinoza-Andaluz, P. Tunestål, M. Andersson
International Journal of Energy Research, 44.6 (2020): 4352-4365
DOI: 10.1002/er.5209

II **A multi-input and single-output voltage control for a polymer electrolyte fuel cell system using model predictive control method**

X.F. Li, **Y.X. Qi**, S.A. Li, P. Tunestål, M. Andersson
International Journal of Energy Research, 45.9(2021): 12854-12863
DOI: 10.1002/er.6616

III **System behavior prediction by artificial neural network algorithm of a methanol steam reformer for polymer electrolyte fuel cell stack use**

Y.X. Qi, J.Y. Wang, L. Wang, M. Andersson
Fuel Cells, (21)2021: 279-289
DOI: 10.1002/fuce.202100006

IV **Polymer Electrolyte Fuel Cell System Level Modelling and Simulation of Transient Behaviour**

Y.X. Qi, M. Espinoza-Andaluz, M. Thern, M. Andersson
eTransportation, 2(2019): 100030
DOI: 10.1016/j.etran.2019.100030

Acknowledgements

This work was carried out at the Heat Transfer Division, Department of Energy Sciences, Faculty of Engineering, Lund University, Sweden. It was sponsored by the Chinese Scholarship Council. The financial support received from ÅForsk (17-331) is also gratefully acknowledged.

I am very grateful to my main supervisor Martin Andersson. His critical thinking, academic confidence, and hard work have helped me grow over the past four years. I am also thankful to my co-supervisor Mayken Espinoza Andaluz for his great advice and patient correction on my papers. I would like to thank my co-supervisors Marcus Thern and Lei Wang as well for all the support I received from them.

Next, I would like to express my gratitude to my co-authors Xiufei Li and Jingyu Wang for our fascinating collaboration. Several interesting discussions with Professor Per Tunestål are also acknowledged.

Last but not least, I would like to thank all my colleagues and administrators at the Department of Energy Sciences for the pleasant working environment and all their cooperation.

Nomenclature

Variables

$\boldsymbol{A^d}$, $\boldsymbol{B^d}$, $\boldsymbol{C^d}$	state-space matrices in discrete-time
$\boldsymbol{r}$	control reference
$\boldsymbol{r}(t)$	reference at time step t
$\boldsymbol{u}_{lb}$	lower bound of input $\boldsymbol{u}$,
$\boldsymbol{u}_{ub}$	upper bound of input $\boldsymbol{u}$
$\boldsymbol{x}$, $\boldsymbol{u}$, $\boldsymbol{y}$	state vector
$\boldsymbol{x}(t)$	initial state at time step t
$\boldsymbol{x}_{init}$	the latest measured value
$\boldsymbol{x}_{lb}$	lower bound of state $\boldsymbol{x}$
$\boldsymbol{x}_{ub}$	upper bound of state $\boldsymbol{x}$
$\dot{m}_{H_2,in}$	hydrogen inlet mass flow rate (kg/s)
$\dot{m}_{H_2,out}$	hydrogen outlet mass flow rate (kg/s)
$\dot{m}_{H_2,rea}$	hydrogen consumption rate (kg/s)
$\dot{m}_{O_2,in}$	oxygen inlet mass flow rate (kg/s)
$\dot{m}_{O_2,out}$	oxygen outlet mass flow rate (kg/s)
$\dot{m}_{O_2,rea}$	oxygen consumption rate (kg/s)
$\dot{q}_{cool}$	heat flow rate generated from the cooling method (J/s)
A	membrane active area (cm^2)

A, B, C	are state space model parameters varying with time t
C	equivalent capacitance of the system (F)
C_S	total surface concentration of specific site (mol/m^2)
C_{O_2}	oxygen concentration (mol/cm^3)
$C_{p,air}$	air specific heat (J/(kg K))
$c_{p,body}$	average specific heat of cell body (J/(K kg))
E_a	activation energy (J/mol)
E_{nernst}	reversible voltage (V)
F	Faraday constant (C/mol)
F_{sH_2}	molar flow rate of the hydrogen in the shell side (mol/s)
F_{ti}	molar flow rate for each i component in the tube side (mol/s)
H_p	predictive horizon length
H_u	control horizon length
I	current (A)
i	actual current density (A/cm^2)
J_{H_2}	hydrogen permeation flux (mol/(m^2 s))
J_{max}	maximum current density (A/cm^2)
K_{1-14}	hydrogen permeation parameters (1/Pa)
k_{1-3}	kinetic constant
$k_{conv,amb}$	reciprocal of thermal resistance (W/K)
$k_{down,an}$	anode outlet mass flow rate coefficient (kg/(s atm))
$k_{up,an}$	anode inlet mass flow rate coefficient (kg/(s atm))
l	membrane thickness (μm)
m_{body}	cell body mass (kg)

M_{H_2}	hydrogen molar mass (g/mol)
m_{H_2}	hydrogen mass (kg)
m_{O_2}	oxygen mass (kg)
n_{cell}	cell number
P_{atm}	ambient pressure (atm)
P_{H_2}	hydrogen partial pressure (atm)
P_{O_2}	oxygen partial pressure (atm)
$P_{s,an}$	hydrogen source pressure (atm)
Q, R	weight-tuning-parameters
R_1	membrane reactor tube radius (m)
R_a	equivalent resistance (Ω)
R_C	equivalent contact resistance to electron conduction (Ω)
R_m	membrane resistance (Ω)
T_{amb}	ambient temperature (K)
T_{stack}	stack temperature (K)
V_{act}	activation voltage drop (V)
V_{con}	concentration voltage drop (V)
V_{FC}	output voltage of the PEFC stack (V)
V_{ohmic}	ohmic voltage drop (V)
W	air mass flow rate (kg/s)
R_2	shell tube radius (m)
S_g	surface area of reforming catalyst (m^2/kg)

Greek letter

β_c	correction factor
β	parametric coefficient (V)

$\Delta H_{R,T}$	lower heating value of hydrogen (J/Kg)
ΔT	temperature difference between the inlet air temperature and outlet air temperature through the fuel cell stack (K)
η_j	effectiveness factor
λ	adjustable parameter
ν_{ij}	stoichiometric coefficient
ρ_{air}	air density (kg/m^3)
ρ_B	reforming catalyst density (kg/ m^3)
ρ_m	membrane resistivity (Ω cm)
ξ	semi-empirical coefficient

Abbreviation

BP	back propagation
FCs	fuel cells
IEA	International Energy Agency
MPC	model predictive control
MR	membrane reactor
MSR	methanol steam reforming
NNAs	neural network algorithms
PEFC	polymer electrolyte fuel cell

Abstract

This thesis focuses on the modelling and controlling of polymer electrolyte fuel cell (PEFC) systems. A system level dynamic PEFC model has been developed to test the system performance (output voltage, reactants gas partial pressures, and stack temperature) for different operating conditions. The simulation results are in good agreement with the experimental data, which indicates that the PEFC model is well qualified to capture the dynamic performance of the PEFC system. Controlling strategies play a significant role in improving the fuel cell system's reliability. Novel model predictive control (MPC) controllers and proportional–integral–derivative (PID) controllers are proposed and implemented in different PEFC systems to control voltage and regulate temperature to enhance system performance. MPC controllers show superior performance to PID controllers in tracking the reference value, with less overshoot and faster response. A novel hydrogen selective membrane reactor (MR) is designed for methanol steam reforming (MSR) to produce fuel cell grade hydrogen for PEFC stack use. The backpropagation (BP) neural network algorithm is applied to find the mapping relation between the MR's operating parameters and the PEFC system's output performance. Simulation results show that the BP neural network algorithm can well predict the system behaviour and that the developed mapping relation model can be used for practical operation guidance and future control applications.

Popular Science Summary

In 2020, the International Energy Agency (IEA) forecasts that world energy demand will increase 19% by 2040. However, traditional fossil fuels are both limited resources and the main drivers for severe environmental damage and health issues. Fuel cells (FCs), by contrast, are environmentally friendly electrochemical devices that convert chemical energy from reactants directly into electricity with water and heat as by-products when hydrogen is used as the fuel. Of the different types of FCs, polymer electrolyte fuel cells (PEFCs) show great promise as an alternative power source with a wide range of applications in transportation, stationary engines, and portable and emergency backup power owing to their low operating temperature, high power density and fast start-up. However, there is still a long way to go before the PEFC technology can dominate the market. Improved cell performance is the key to promoting the widespread use of PEFCs.

From a research point of view, modelling appears a suitable tool to predict the behaviour of PEFCs on different scales and provide solutions to fuel cell problems efficiently. Modelling on a system scale can simulate PEFCs' performance under a wide range of operating conditions and improve system integration, control algorithms design and system performance optimization.

Reliable and effective control strategies also play a significant role in improving the performance of PEFC systems, and thus there is intense interest in developing robust and effective control methods. One such method is model predictive control (MPC), an advanced process control method widely used in academic fields and industry due to its high robustness and outstanding performance. The major advantage of MPC is that it can directly deal with state constraints during transient operations, which makes it a good choice for PEFC systems whose systemic parameters need to be carefully coordinated within suitable ranges.

To provide quality performance, PEFC system needs high purity hydrogen as fuel. Methanol steam reforming (MSR) is the most attractive on-board hydrogen production method because of its low cost and high safety. Hydrogen selective membrane reactors are a major solution used for MSR, because they allow the hydrogen to permeate from the reforming zone to the shell tube through the membrane, thus delivering high purity hydrogen.

Instead of building complicated mathematical models, it is possible to use neural network algorithms (NNAs), which are powerful tools that can be used to learn and store the mapping relations of a set of inputs and outputs. Of the wide range of neural network methods, the backpropagation (BP) method receives the

most attention because of its strong self-learning and adaptive capabilities. BP method has been widely used in fuel cell systems for parameter tuning, model design, degradation prediction, control parameters exploration, performance prediction, voltage tracking, and ageing prognosis.

To address each key point illustrated above, in this work, a system level PEFC model was developed that can predict the transient behaviour of the system, that is, the output voltage, reactant pressure and stack temperature under various load conditions. Several novel MPC controllers were developed and implemented in different PEFC systems with applications in voltage regulation and stack temperature control. Moreover, a novel membrane reactor was designed to generate hydrogen for PEFC system use. The BP algorithm is employed to find the mapping relation between the operating parameters of the membrane reactor and the PEFC system output performance for practical operation guidance and future control applications.

Chapter 1

Introduction

This chapter presents an overview of the thesis. The fuel cells introduction, the significant contribution PEFCs can make to solving the energy crisis, the research objectives, the adopted modelling and controlling methodology, and the thesis scope are are all discussed to give readers an insight into the research project.

1.1 Brief Introduction on Fuel Cells

Fuel cells are electrochemical devices that convert the chemical energy of a fuel (including fuels from various renewable energy sources) and an oxidizing agent directly and efficiently into electricity through a pair of redox reactions, usually with water, heat and carbon dioxide as by-products. These by-products are much less harmful than those from internal combustion engines (ICEs) [1]. Not only can FCs contribute to reducing pollutant emissions and our reliance on fossil fuels, but they are also compact in size and noiseless, and can be employed in applications ranging from a few watts to several gigawatts [2]. FCs are made up of three adjacent segments: an anode, an electrolyte, and a cathode. Based on the electrolyte used, FCs can be categorized as: alkaline fuel cells (AFCs), phosphoric acid fuel cells (PAFCs), polymer electrolyte fuel cells (PEFCs), molten carbonate fuel cells (MCFCs) and solid oxide fuel cells (SOFCs) [3].

Of the various types of FCs, PEFCs are regarded as the prime alternative power sources for transportation, stationary, and portable applications thanks to their low operating temperature, simple construction, high power density, and fast start up [4]. PEFCs use a proton conductive polymer membrane as the electrolyte, which is sandwiched between two electrodes (the anode and cathode). The interface between the electrode and the electrolyte membrane is the catalyst

layer where the electrochemical reactions happen. A schematic diagram of a PEFC configuration and its basic working principles is shown in Figure 1.1 [5]. Hydrogen is fed to the anode and then split into protons and electrons at the catalyst layer. Meanwhile, oxygen is delivered to the cathode side. The protons transfer through the polymer electrolyte membrane to the cathode side. While, the electrons transfer through the external load circuit to the cathode side. At the catalyst layer between the membrane and cathode, oxygen reacts with protons and electrons to form water. And because of the movement of electrons, a current is produced. The hydrogen oxidation reaction (HOR), oxygen reduction reaction (ORR), and the overall reaction can be represented as follows:

$$\mathrm{H_2} \longrightarrow 2\,\mathrm{H^+} + 2\,\mathrm{e^-} \qquad \text{(HOR)}$$
$$(1/2)\,\mathrm{O_2} + 2\,\mathrm{H^+} + 2\,\mathrm{e^-} \longrightarrow \mathrm{H_2O} \qquad \text{(ORR)}$$
$$\mathrm{H_2} + (1/2)\,\mathrm{O_2} \longrightarrow \mathrm{H_2O}$$

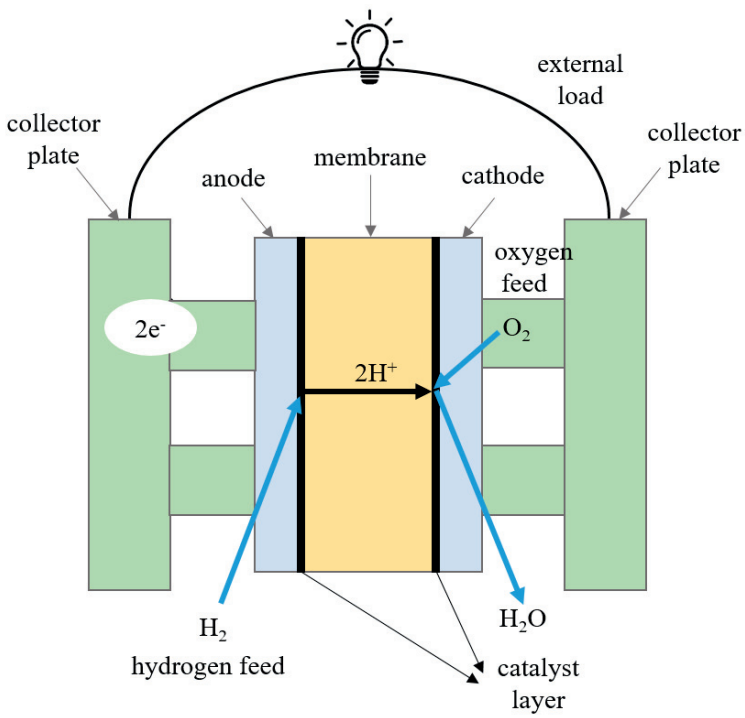

Figure 1.1: Schematic diagram of a PEFC configuration [5].

1.2 Research Objectives

The development of modern civilization and population growth have resulted in dramatic increase in the demand for energy, which currently supplied by the combustion of fossil fuels. This is problematic given that fossil fuels are a limited resource that is rapidly depleting. Moreover, fossil fuels also contribute to severe environmental problems including global warming, sea level rise, ozone layer degradation, and pollution [5]. Currently, the main devices used for energy extraction and conversion are ICEs. Such engines release great amounts of greenhouse gases (GHGs) during operation, with adverse impacts on environment, and their efficiency is limited by the Carnot cycle [6]. PEFCs appear to offer a very promising alternative power source due to their high power density and environmental friendly feature.

According to the 2020 "PEMFCs (Proton Exchange Membrane Fuel Cells) - Global Market Trajectory & Analytics" Report, the value of the global market for PEFCs was estimated at $4.6 billion in the year 2020 and was expected to reach $16.3 billion by 2027 at a compound annual growth rate (CAGR) of 19.8% as shown in Figure 1.2 [7]. Although PEFCs are projected to continue making progress in subsequent years, their performance degradation and cost remain the two major bottlenecks for its commercialization [8]. A PEFC is a complex, nonlinear and highly coupled system that involves rather complicated phenomena, making it hard to analyse and study in situ. Thus, the modelling of PEFCs serves as a powerful tool to simulate cell operation and forecast performance under different load cycles, which can help to direct the manufacturing process and eventually save production and development time and cost [9–11]. Numerous studies have focused on the modelling of PEFCs for different purposes. Based on their scales, the modelling of PEFCs can be categorized as system scale, component scale, flow/diffusion scale, material structure/interface scale, and functional material scale models [12, 13]. System level modelling can be applied to develop and optimize fuel cell system design, devise control algorithms, and optimize fuel stack parameters, which can ultimately help to prolong the service life and enhance fuel cell performance [14]. So far, only limited research has focused on the system level modelling of PEFCs for specific purposes such as, constructing model libraries, characterizing system transient behaviour, optimizing operation, designing control systems and testing durability [15–20]. Though earlier studies have laid a solid foundation for PEFC system modelling, a comprehensive model that incorporates the mixed effects of stack temperature, reactant flow, and electric capacitance with the aim of predicting system performance under various operation conditions is still much needed. Therefore, this thesis reports on the development of a system level dynamic

PEFC model that can characterize the system dynamic behaviour under different load cycles.

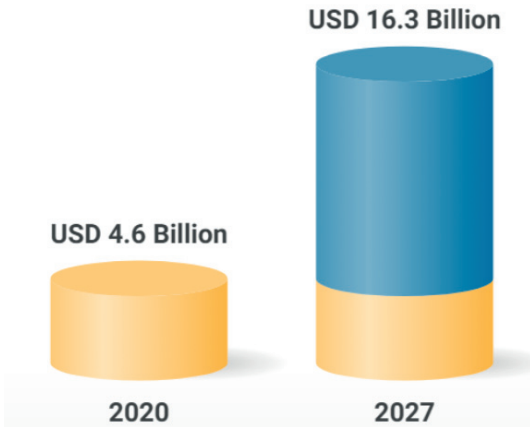

Figure 1.2: Global market for PEFC [7].

Control strategies play a significant role in improving PEFC system performance. Extensive research has been devoted to developing efficient and robust control algorithms that can be implemented in PEFC systems for various applications. Sliding mode control, nonlinear control, generalized predictive control (GPC), neural optimal control (NOC), feedback linearization control, linear quadratic regulator (LQR) approach, cascaded extremum seeking control algorithm, proportional-integral-derivative controller (PID), adaptive control, model predictive control and fuzzy logic control have all been employed in PEFC systems for specific uses. These uses include oxygen starvation avoidance, power consumption reduction, minimum fuel consumption points tracking, voltage and power regulation, stability improvement, reactant partial pressure maintenance, efficiency maximization, temperature control, and air feed control [21–27]. Previous studies have paved a solid path for researchers and manufacturers to improve cell performance. However, more effective and reliable controllers are still needed because of the complexity and nonlinearity of PEFC systems. MPC controllers are an advanced method of process control and are widely used in academic and industrial fields because of their stability, robustness, constraint satisfaction, and tractable computation for linear and nonlinear systems [28, 29]. An MPC controller can anticipate future events while allowing the current time slot to be optimized. Its effectiveness in dealing with input and state constraints makes it very suitable for PEFC systems since the fuel cell system has many constraints on the input parameters [30]. MPC controllers have been used in PEFC systems for temperature control, air flow control, prevention of fuel starvation, optimum power generation, hydrogen consumption minimization and efficiency improve-

ment [31–34]. Therefore, this thesis reports on the design and implementation of novel MPC controllers in PEFC system models for applications in temperature control and voltage regulation.

The lack of high purity hydrogen sources poses another challenge that limits the application of PEFC systems due to possible poisoning. Therefore, intensive research is being done on the production of fuel cell grade hydrogen. Given the difficulty of storing and transporting hydrogen, much attention has been paid to on-board hydrogen generation [35, 36]. A popular method of doing this involves reforming alcohols and hydrocarbons, which allows hydrogen production in situ. Hydrogen can be produced using various fuels including glycerol, ethanol, and even animal waste [37–41]. Methanol is an attractive option due to its low operating temperature, high hydrogen to carbon ratio, lower sulphur content, and absence of a strong C–C bond. Moreover, it can be produced on a large scale from different sources [42–45]. However, CO forms as a co-product during methanol steam reforming and poisons the electrolyte membrane of the PEFC system when CO level reaches more than 10 ppm. Thus, much research has focused on the pre-treatment of reformate gas before sending it to a fuel cell. The possible pre-treatments include combining the reformer with a water gas shift (WGS) reactor, preferential CO oxidation (PROX) reactor, or pressure swing adsorption unit [46–48]. However, these combination units can be difficult to carry and are not suitable for automotive fuel cell applications [49]. A membrane reactor fitted to a methanol steam reformer with a hydrogen selective membrane is an attractive option to generate high purity hydrogen because it allows only the hydrogen to permeate through the membrane from the reforming zone to the permeation zone [50]. A catalyst is required for methanol steam reforming, usually copper-based and palladium-based catalysts are used [36]. A Pd/Ag membrane is widely used for the hydrogen selective membrane because of its infinite permeation selectivity for hydrogen [51]. Therefore, in this thesis we report on the design of a novel hydrogen selective membrane reactor for methanol steam reforming to generate fuel cell grade hydrogen.

The permeated hydrogen can be used as the fuel source for the PEFC system after condensation. However, the operating parameters of the membrane reactor greatly affect its hydrogen production, which leads to variations in PEFC system performance. In addition, both the membrane reactor and the PEFC model involve complicated nonlinear mathematical equations, which makes it difficult to integrate system design and control applications. There is thus a need for a simple but accurate model mapping the relation between the membrane reactor's operating conditions and the PEFC system performance. Neural network algorithms (NNAs) are powerful tools that endeavour to recognize the

hidden patterns and correlations in a set of raw data through a process that mimics the way the human brain operates [52]. The backpropagation (BP) algorithm is one of the most popular and widely used NNAs due to its self-learning and self-adaptive capability, nonlinear mapping capability, high fault tolerance, effective training process and simple structure [53]. Therefore, in this thesis, the BP method is used to find the mapping relation model between the membrane reactor's prime operation parameters and the PEFC system's output performance.

The main objective of this thesis is to study the transient properties of a PEFC system under different load conditions, using controlling algorithms to improve system performance and reliability. Achieving this objective requires the following steps:

- Developing a system level dynamic PEFC model to capture the system performance under different operating conditions, using parameters such as output voltage, stack temperature and reactant gas pressure.
- Designing novel MPC and PID controllers and implementing them in the PEFC system for temperature and voltage control.
- Proposing an effective methanol steam reformer to provide high purity hydrogen for a PEFC stack, using the BP neural network algorithm to map the relation between the operating parameters of the methanol steam reformer and the fuel cell's output performance for practical production guidance and control applications.

1.3 Methodology

All numerical simulations in this thesis were carried out in Matlab and Simulink. For the PEFCs, a system scale dynamic model based on the governing equations of mass and energy conservation was built in Simulink to study the system's transient behaviour under different operating conditions. For the methanol steam reformer, a series of ordinary differential equations that incorporate three reactions, namely steam reforming of methanol, methanol decomposition, and water gas shift reactions were solved using the ode15s solver in Matlab to produce fuel cell grade hydrogen. The MPC controllers were developed in Simulink with the tuning method of linearizing the original PEFC system model.

1.4 Thesis Outline

Following this brief introduction in **Chapter 1**, **Chapter 2** presents the modelling methodology of the PEFC system, the control algorithms, the membrane reactor model, and the BP neural network algorithm. **Chapter 3** gives the results of the modelling and controlling of PEFC systems, the membrane reactor's performance, and the BP neural network method's prediction behavior. **Chapter 4** presents the conclusions and outlines future work. Finally, **Chapter 5** briefly summarizes all the related papers, which are attached at the end of this thesis.

Chapter 2

Methodology analysis

In this chapter, the PEFC system modelling methodology, the MPC controller algorithm, the membrane reactor modelling method, and the BP neural network algorithm are explained in detail.

2.1 PEFC System Model Methodology

2.1.1 Pre-analysis of PEFC model development

The PEFC model developed in this work is at the system level and the focus is on the macro performance of the PEFC system. Thus, the details of fluid flow in the porous area, the temperature distribution across the cell area, and the reaction distribution on the catalyst layer are not considered. The water generated in the cathode may involve a two-phase flow pattern, but that is beyond the scope of this thesis, thus is not considered either. In the operating temperature range of a PEFC system (223–373 K), we may assume the reactant gases follow the ideal gas law, i.e., comparing the operating temperature to the critical temperature of each component. In addition, the performance of the PEFC system can be represented by the combined effect of each cell in the system.

2.1.2 Governing equations

There are two main types of modelling methods for PEFCs, namely, mechanistic (theoretical) modelling and semiempirical modelling. Mechanistic models are usually used to simulate the electrochemical reactions and the mass, species, and charge transfer phenomena occurring within the fuel cell. They are obtained from electrochemical, thermodynamic, and fluid dynamic equations. These mechanistic models are very complex and involve extensive calculations, and it is difficult to obtain the parameters [54]. Unlike mechanistic models, semiempirical

models are able to capture the electrochemical behaviour of a FC without offering deep details of the underlying phenomena. They have a simple structure and require little computational effort to perform the calculations [55, 56]. Therefore, a semiempirical model is developed for the PEFC system in this work.

Voltage formulation

The typical output voltage of a PEFC is usually less than the ideal value due to the activation voltage drop, ohmic voltage drop, and concentration voltage drop across the fuel cell. Thus, to obtain a higher voltage, a number of cells are usually combined in series and the net output voltage of a PEFC is computed as follows [57, 58]:

$$V_{FC} = n_{cell}(E_{nernst} - V_{act} - V_{ohmic} - V_{con}) \tag{2.1}$$

where V_{FC}, n_{cell}, E_{nernst}, V_{act}, V_{ohmic} and V_{con} denote the output voltage of the PEFC (V), cell number, reversible voltage (V), activation voltage drop (V), ohmic voltage drop (V) and concentration voltage drop (V), respectively.

Reversible voltage

The reversible voltage, which is alternatively called open circuit voltage is computed using the Nernst equation that can be expressed as the following equation [57, 58]:

$$\begin{aligned} E_{nernst} = {} & 1.229 - 0.85 * 10^{-3}(T_{stack} - 298.15) \\ & + 4.3085 * 10^{-5} T_{stack} \left[ln(P_{H_2}) + 0.5 ln(P_{O_2})\right] \end{aligned} \tag{2.2}$$

where T_{stack}, P_{H_2} and P_{O_2} are stack temperature (K), hydrogen partial pressure (atm) and oxygen partial pressure (atm), respectively.

Activation voltage drop

The activation voltage drop V_{act} occurs due to the activation of the electrodes. It is dominant in the low current density region and defined as [59]:

$$V_{act} = -\left[\xi_1 + \xi_2 T_{stack} + \xi_3 T_{stack} ln(C_{O_2}) + \xi_4 T_{stack} ln\,(I)\right] \tag{2.3}$$

$$C_{O_2} = \frac{P_{O_2}}{5.08 * 10^6 * exp(\frac{-498}{T_{stack}})} \tag{2.4}$$

where ξ is the semi-empirical coefficient, C_{O_2} is the oxygen concentration (mol/cm^3), and I is the current (A).

Ohmic voltage drop

The ohmic voltage drop V_{ohmic} results from the resistance to the electron transfer through the collecting plates and carbon electrodes, and the resistance to proton transfer through the solid membrane. It is given as [59]:

$$V_{ohmic} = I(R_m + R_C) \tag{2.5}$$

$$R_m = \frac{\rho_m l}{A} \tag{2.6}$$

$$\rho_m = \frac{181.6\left[1 + 0.03(i) + 0.062(T_{stack}/303)^2(i)^{2.5}\right]}{(\lambda - 0.643 - 3 * i)exp(4.18(\frac{T_{stack}-303}{T_{stack}}))} \tag{2.7}$$

where R_m, R_C, ρ_m, l, A, i, λ represent membrane resistance (Ω), equivalent contact resistance to electron conduction (Ω), membrane resistivity (Ω cm), membrane thickness (μm), membrane active area (cm^2), actual current density (A/cm^2) and adjustable parameter related to water content of the membrane, respectively.

Concentration voltage drop

The concentration voltage drop V_{con} is due to the mass transport which affects the concentrations of hydrogen and oxygen, reducing the partial pressure of the these gases. It is determined as [60]:

$$V_{con} = -\beta ln(1 - i/J_{max}) \tag{2.8}$$

where, β is a parametric coefficient (V), and J_{max} denotes the maximum current density (A/cm^2).

Charge double layer

The 'charge double layer' phenomenon plays a significant role in PEFC dynamic performance. Whenever two differently charged materials are in contact, a charge accumulates on their surfaces or a load transfers from one to the other. In a fuel cell, electrons will collect at the electrode surface, and protons will transfer to the electrolyte surface. These electrons and protons at the electrode/electrolyte interface will generate an electrical voltage and the charge layer on this interface (or close to the interface) acts as a storage of electrical charge and energy. In this way, it behaves as an electrical capacitor. If the current changes, it will take a certain period for this charge to build up or dissipate. Therefore, the voltage does not immediately follow the current. It should be noted that this delay only

affects the activation and concentration potentials [61]. The dynamics of fuel cell voltage can be described by a differential equation [62, 63]:

$$\frac{dV_a}{dt} = \frac{I}{C} - \frac{V_a}{R_a C} \tag{2.9}$$

$$R_a = \frac{V_{act} + V_{con}}{I} \tag{2.10}$$

where C and R_a denote the equivalent capacitance of the system (F) and the equivalent resistance (Ω). Thus, the output voltage of the PEFC can be rewritten as:

$$V_{FC} = n_{cell}(E_{nernst} - V_a - V_{ohmic}) \tag{2.11}$$

Reactant flow model

The reactant flow rate at the anode and cathode side greatly affects the effective partial pressures of hydrogen and oxygen, which then directly affect the fuel cell output voltage. At the anode side, hydrogen is delivered to the PEFC system as the fuel. Based on the mass conservation law, the hydrogen mass change rate is related to the hydrogen inlet mass flow rate, hydrogen outlet mass flow rate, and hydrogen consumption rate [16, 64, 65]:

$$\frac{dm_{H_2}}{dt} = \dot{m}_{H_2,in} - \dot{m}_{H_2,rea} - \dot{m}_{H_2,out} \tag{2.12}$$

where m_{H_2}, $\dot{m}_{H_2,in}$, $\dot{m}_{H_2,rea}$, and $\dot{m}_{H_2,out}$ are hydrogen mass (kg), hydrogen inlet mass flow rate (kg/s), hydrogen consumption rate (kg/s) and hydrogen outlet mass flow rate (kg/s), respectively. The hydrogen consumption rate is related to cell number and stack current. The inlet and outlet mass flow rate may be simplified as the traditional nozzle flow rate equation. They can be respectively described as [16, 64, 66]:

$$\dot{m}_{H_2,rea} = \frac{n_{cell} I}{2F} M_{H_2} \tag{2.13}$$

$$\dot{m}_{H_2,in} = k_{up,an}(P_{s,an} - P_{H_2}) \tag{2.14}$$

$$\dot{m}_{H_2,out} = k_{down,an}(P_{H_2} - P_{atm}) = k_a(P_{H_2} - P_{atm})M_{H_2} \tag{2.15}$$

where F, M_{H_2}, $k_{up,an}$, $P_{s,an}$, $k_{down,an}$, k_a and P_{atm} represent the Faraday constant (C/mol), hydrogen molar mass (g/mol), anode inlet mass flow rate coefficient (kg/(s atm)), hydrogen source pressure (atm), anode outlet mass flow rate coefficient (kg/(s atm)), anode outlet molar flow rate coefficient (mol/(s atm)), and ambient pressure (atm), respectively.

At the cathode side, oxygen is delivered to the PEFC system. As on the anode side, based on the mass conservation law, the oxygen mass change rate is related to the oxygen inlet mass flow rate, oxygen outlet mass flow rate, and oxygen consumption rate [16, 64, 65]:

$$\frac{dm_{O_2}}{dt} = \dot{m}_{O_2,in} - \dot{m}_{O_2,rea} - \dot{m}_{O_2,out} \tag{2.16}$$

where m_{O_2}, $\dot{m}_{O_2,in}$, $\dot{m}_{O_2,rea}$, and $\dot{m}_{O_2,out}$ are oxygen mass (kg), oxygen inlet mass flow rate (kg/s), oxygen consumption rate (kg/s) and oxygen outlet mass flow rate (kg/s), respectively. The oxygen consumption rate is related to cell number and stack current. The inlet and outlet mass flow rate may be simplified as the traditional nozzle flow rate equation. They can be respectively described as [16, 64, 66]:

$$\dot{m}_{O_2,rea} = \frac{n_{cell} I}{4F} M_{O_2} \tag{2.17}$$

$$\dot{m}_{O_2,in} = k_{up,ca}(P_{s,ca} - P_{O_2}) \tag{2.18}$$

$$\dot{m}_{O_2,out} = k_{down,ca}(P_{O_2} - P_{atm}) = k_c(P_{O_2} - P_{atm})M_{O_2} \tag{2.19}$$

where M_{O_2}, $k_{up,ca}$, $P_{s,ca}$, k_c and $k_{down,ca}$ represent the oxygen molar mass (g/mol), cathode inlet mass flow rate coefficient (kg/(s atm)), oxygen source pressure (atm), cathode outlet molar flow rate coefficient (mol/(s atm)) and cathode outlet mass flow rate coefficient (kg/(s atm)), respectively.

However, when air is supplied at the cathode instead of pure oxygen, the cathode volume model is redefined as equations 2.20-2.24.

$$\dot{m}_{O_2,in} = 0.21 * \dot{V}_{air} * \rho_{O_2} \tag{2.20}$$

$$\dot{m}_{O_2,out} = k_{down,ca} \frac{m_{O_2}}{m_{O_2} + m_{N_2}} (P_{ca} - P_{amb}) \tag{2.21}$$

$$\frac{dm_{N_2}}{dt} = \dot{m}_{N_2,in} - \dot{m}_{N_2,out} \tag{2.22}$$

$$\dot{m}_{N_2,in} = 0.79 * \dot{V}_{air} * \rho_{N_2} \tag{2.23}$$

$$\dot{m}_{N_2,out} = k_{down,ca} \frac{m_{N_2}}{m_{O_2} + m_{N_2}} (P_{ca} - P_{amb}) \tag{2.24}$$

here $\dot{V}_{air}$, ρ_{O_2}, ρ_{N_2}, m_{N_2}, $\dot{m}_{N_2,in}$, $\dot{m}_{N_2,out}$, and P_{ca} are air volume flow rate (m^3/s), oxygen density (kg/m^3), nitrogen density (kg/m^3), nitrogen mass (kg), inlet nitrogen mass flow rate (kg/s), outlet nitrogen mass flow rate (kg/s), and cathode pressure (atm), respectively.

Thermal model

The stack temperature greatly affects cell performance. Based on the energy conservation law, the internal energy change rate of a cell body is related to the heat added to and the work done on the cell body, which can be expressed as:

$$m_{body}c_{p,body}\frac{dT}{dt} = \Delta H_{R,T}\frac{n_{cell}I}{2F}M_{H_2} - n_{cell}V_{cell}I + k_{conv,amb}(T_{amb} - T_{body}) \quad (2.25)$$

where m_{body}, $c_{p,body}$, $\Delta H_{R,T}$, $k_{conv,amb}$ and T_{amb} represent cell body mass (kg), average specific heat of cell body (J/(K·kg)), the lower heating value of hydrogen (J/Kg), reciprocal of thermal resistance (W/K) and ambient temperature (K), respectively.

2.2 MPC Controller Methodology

2.2.1 Introduction of MPC controller

MPC is an advanced process control method that is used to control a process while satisfying a set of constraints. It is a systematic model-based approach that uses dynamic models of the process. The dynamic models are most often linear empirical models obtained by system identification and used to predict the future behaviour of the controlled system and generate a control vector that minimizes a particular cost function over the prediction horizon in the presence of disturbances and constraints. At each sampling instant, an open-loop optimization problem is solved. Only the first element of the computed control vector is applied to the plant, and the rest of the solution is discarded. At the next time instant, the optimization parameters are updated by means of an output feedback, a new open-loop optimization is performed, and the prediction horizon is shifted forward one step. This is usually called the receding horizon strategy [67]. MPC can be applied for both single-input single-output (SISO) and multi-input multi-output (MIMO) linear and nonlinear processes. The primary advantage of MPC is its ability to deal with constraints, which are included in the optimization problem. Another key selling point of MPC is that it allows the current time slot to be optimized, while keeping future time slots in reserve [68]. The MPC method has been applied in fields such as residential building energy management, air–fuel ratio control in combustion engines, path tracking control, helicopter trajectory tracking, changing economic criteria , tracking zone regions, and health care [69–74].

2.2.2 Adaptive MPC Controller

A traditional linear MPC predicts future behaviour using a linear-time-invariant (LTI) dynamic model. These predictions are never close enough in practical cases. Thus a key tuning objective is to make the MPC insensitive to prediction errors, which is sufficient for robust controller performance in many applications. However, if a plant is strongly nonlinear like the PEFC system, the MPC performance may become unacceptable because of the degradation of the LTI prediction accuracy. Adaptive MPC can address this degradation by adapting the prediction model for changing operating conditions. Adaptive MPC uses a fixed model structure but allows the model parameters to evolve over time. Ideally, whenever the controller requires a prediction (at the beginning of each control interval), it uses a model appropriate for the current conditions. At each control interval, the adaptive MPC controller updates the plant model and nominal conditions. Once updated, the model and conditions remain constant over the prediction horizon [75–77].

To clarify, the main focus of the control algorithm in this thesis is the MPC method. However, a PID controller is also developed and implemented in the PEFC system for different control purposes. PID is the most commonly used control method in industry. It can handle most problems and achieve acceptable performance. PID is also very easy to implement and is always the primary choice if a control problem can be solved by PID. Therefore, a PID controller is used as the baseline.

2.2.3 Temperature control of PEFC system by adaptive MPC

Cooling system of PEFC system

The stack temperature can greatly affect the performance of a PEFC system. A too high temperature can dehydrate the polymer electrolyte membrane and decrease the proton conductivity. On the other hand, a too low temperature can slow down the electrochemical reaction rate and the water inside the cell system will condense, causing flooding [78, 79]. Therefore, it is essential to maintain the optimal PEFC temperature. Liquid and airflow coolant circuits are two typical cooling systems used in PEFC systems to remove excess heat and keep the operating temperature within the desired range. The current work employs an airflow cooling method because of its simple design and convenient operation [80]. The schematic diagram of the airflow coolant circuit is presented in Figure 2.1. It can be seen that the air flows through the cooling channels, removing heat from the surface of the fuel cell stack.

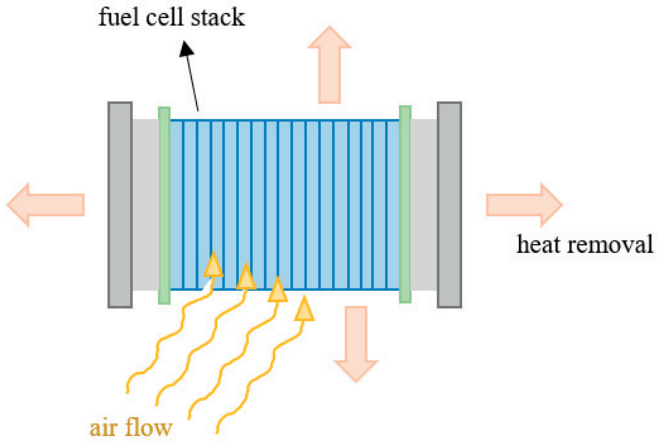

Figure 2.1: Airflow coolant circuit schematic.

Since a certain amount of heat will be removed from the PEFC system by the airflow coolant circuit, the thermal model (equation 2.25) can be rewritten as follows:

$$m_{body}c_{p,body}\frac{dT}{dt} = \Delta H_{R,T}\frac{n_{cell}I}{2F}M_{H_2} - n_{cell}V_{cell}I + k_{conv,amb}(T_{amb} - T_{body}) - \dot{q}_{cool} \tag{2.26}$$

$$\dot{q}_{cool} = C_{p,air}W\Delta T \tag{2.27}$$

$$W = CFM \times \rho_{air} \tag{2.28}$$

where $\dot{q}_{cool}$, $C_{p,air}$, W, ΔT and ρ_{air} are heat flow rate generated from the cooling method (J/s), air specific heat (J/(kg K)), air mass flow rate (kg/s), temperature difference between the inlet air temperature and outlet air temperature through the fuel cell stack (K) and air density (kg/m^3), respectively. Note that 1 CFM =0.028 m^3/min.

Control objective

Normally, the operating temperature of a PEFC system is between 60–80 °C for stable operation. Generally, it is kept below 80 °C. Therefore, the control objective in this paper is to keep the system temperature at 70 °C (343 K) by regulating the air flow rate, which is a SISO control scheme.

Control system scheme

The control scheme of the PEFC temperature with MPC and PID controllers is presented in Figure 2.2 and Figure 2.3 respectively. For the MPC controller, the input contains the reference temperature, current, actual stack temperature, as well as the state vector. For the PID controller, the difference between the desired temperature and the actual temperature is set as its input. A trial and error method is used to tune the PID controller. The tuning method for MPC is given explicitly in the next paragraph.

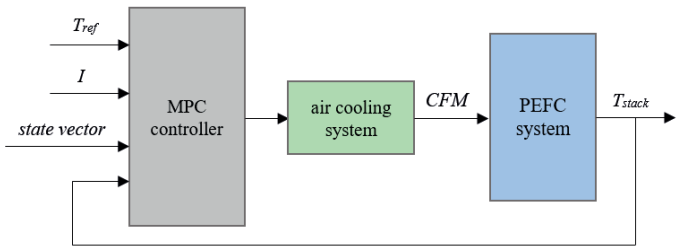

Figure 2.2: Temperature control by MPC method.

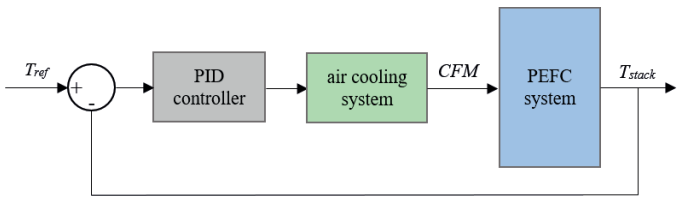

Figure 2.3: Temperature control by PID method.

Tuning method of MPC controller for temperature regulation

Considering a linear state space model that can be represented as:

$$\dot{\boldsymbol{x}}(k) = A(t)\boldsymbol{x}(k) + B(t)\boldsymbol{u}(k) \tag{2.29}$$

$$\boldsymbol{y}(k) = C(t)\boldsymbol{x}(k) \tag{2.30}$$

where $\boldsymbol{x}$, $\boldsymbol{u}$, and $\boldsymbol{y}$ are the state vector, input vector and output vector, respectively. A, B and C are state space model parameters varying with time t.

The MPC will solve a quadratic programming (QP) problem to obtain the optimal control inputs at each time step t based on the following equation:

$$\min_{\boldsymbol{u}} \left(\sum_{k=2}^{H_p} \|\boldsymbol{y}(k) - \boldsymbol{r}(t)\|_Q + \sum_{k=1}^{H_u} \|\boldsymbol{u}(k)\|_R \right) \tag{2.31}$$

subject to equations 2.29 and 2.30 with the following constraints:

$$\boldsymbol{x}_{lb} \leq \boldsymbol{x}(k) \leq \boldsymbol{x}_{ub} \tag{2.32}$$

$$\boldsymbol{u}_{lb} \leq \boldsymbol{u}(k) \leq \boldsymbol{u}_{ub} \tag{2.33}$$

$$k = 1, 2...H_p \tag{2.34}$$

where $\boldsymbol{r}(t)$ is the reference at time step t. Q and R are both weight tuning parameters for reference tracking and control inputs; $\boldsymbol{x}(t)$ is the initial state at time step t; $\boldsymbol{x}_{lb}$ and $\boldsymbol{x}_{ub}$ are the lower bound and upper bound of state $\boldsymbol{x}$, respectively; $\boldsymbol{u}_{lb}$ and $\boldsymbol{u}_{ub}$ are lower bound and upper bound of input $\boldsymbol{u}$, respectively; H_p is the predictive horizon length and H_u is the control horizon length.

The solved $\boldsymbol{u}(1)$ will be set as system inputs of time step t. In the next time step, a new QP problem will be solved again and new control inputs are obtained. Since A, B and C depend on a set of varying parameters, it is also known as the linear parameter-varying (LPV) model, and the corresponding MPC problem is linear time varying model predictive control, LPV-MPC.

To represent the PEFC in the desired linear state space model, we set:

$$\boldsymbol{x} = \begin{bmatrix} T_{stack} \\ V_{cell} \\ 1 \end{bmatrix} \tag{2.35}$$

$$\boldsymbol{u} = \begin{bmatrix} CFM \end{bmatrix} \tag{2.36}$$

$$\boldsymbol{y} = \begin{bmatrix} T_{stack} \end{bmatrix} \tag{2.37}$$

Based on equations 2.2-2.11 and 2.26-2.28 the following expressions are obtained:

$$\begin{aligned} \dot{T}_{stack} = \frac{1}{m_{st} c_{p,st}} (&-k_{conv,amb} T_{stack} - I n_{cell} V_{cell} + \Delta H_{R,T} \frac{n_{cell} I}{2F} M_{H_2} \\ &+ k_{conv,amb} T_{amb} - \rho_{air} CFM \times C_{p,air} \Delta T V_{cell}) \end{aligned} \tag{2.38}$$

$$\dot{V}_{cell} = (\frac{I/C}{V_{act}+V_{con}})(-0.85\times10^{-3}+4.308\times10^{-5}(lnP_{H_2}+0.5lnP_{O_2}))T_{stack} - V_{cell} + (-(V_{act}+V_{con}) - V_{ohm} + 1.229 + 0.85\times10^{-3}\times298.5) \tag{2.39}$$

The last element 1 in the state vector $\boldsymbol{x}$ is used to take the constant term in the equation into account. Correspondingly, the state space vectors A, B and C in equations 2.29 and 2.30 can be written as follows:

$$A(t) = \begin{bmatrix} -k_{conv,amb}/m_{st}c_{p,st} & -In_{cell}/m_{st}c_{p,st} & \frac{\dot{q}_{tot}+k_{conv,amb}T_{amb})}{m_{st}c_{p,st}} \\ A_{21} & -(I/C)/(V_{act}+V_{con}) & A_{23} \\ 0 & 0 & 0 \end{bmatrix} \tag{2.40}$$

$$\dot{q}_{tot} = \Delta H_{R,T}\frac{n_{cell}I}{2F}M_{H_2} \tag{2.41}$$

$$A_{21} = ((I/C)/(V_{act}+V_{con}))(0.85\times10^{-3}+4.3085\times10^{-5}(lnP_{H_2}+0.5lnP_{O_2})) \tag{2.42}$$

$$A_{23} = ((I/C)/(V_{act}+V_{con}))(-(V_{act}+V_{con})-V_{ohm}+1.229+0.85\times10^{-3}\times298.15) \tag{2.43}$$

$$B(t) = \begin{bmatrix} (1/m_{st}c_{p,st})C_{p,air}(-\rho_{air})\times CFM\times\Delta T \\ 0 \\ 0 \end{bmatrix} \tag{2.44}$$

$$C(t) = \begin{bmatrix} 1 & 0 & 0 \end{bmatrix} \tag{2.45}$$

At each time step t, the QP problem considering the state space model is solved and the first element of the solved input sequence is applied to the system. In our MPC setting, the predictive horizon H_P is 10 and control horizon H_U is 2. The weight Q is set to 100 and R is 0.1. The lower bound and upper bound of input variable CFM are 0 and 100, respectively, and there are no constraints on the state vector.

2.2.4 Voltage control of PEFC system by adaptive MPC

Control objective

A steady output voltage is an important criterion for evaluating a fuel cell system's reliability as an alternative power source in practical applications [81]. In this section, it is assumed that the PEFC system can be utilized as a steady power source for an electric vehicle. Reactant gas flow rates can greatly affect the hydrogen and oxygen partial pressures in the gas channels, thus leading to

a variation in the PEFC system output voltage [82, 83]. Hence, the control objective is to stabilize the PEFC system voltage at a desired value by regulating its input hydrogen and air flow rates at the same time, which is a multi-input single-output (MISO) control problem.

Control system scheme

The control schemes of the MPC controller and PID controller are presented in Figure 2.4 and Figure 2.5 respectively. It can be seen that the input of the MPC controller contains the reference voltage, the actual voltage, and state vector, which is obtained by linearizing the controlled system. For the PID controller, the difference between the reference voltage and the actual output voltage is set as the input. Two PID controllers are employed, one for hydrogen regulation and one for air flow rate regulation. The MPC can handle a multi-input control problem without implementing extra MPC controllers. The measurement errors which may occur in practical operation are represented as a noise signal applied to the actual output voltage during the whole control process to make the simulation closer to the practical experience. The trial and error method is applied to tune the PID controller. The MPC tuning method is given explicitly in the next paragraph.

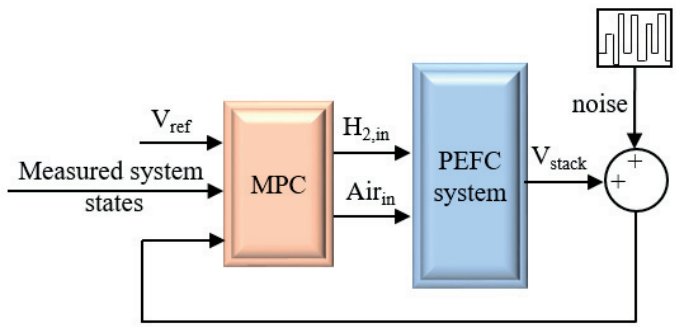

Figure 2.4: MPC control scheme.

Tunning method by MPC controller for voltage regulation

The tuning of the MPC starts with the linearization of the original PEFC model. Differentiating both sides of equation 2.11:

$$\dot{V}_{FC} = n_{cell} \times (\dot{E}_{nernst} - \dot{V}_a - \dot{V}_{ohmic}) \tag{2.46}$$

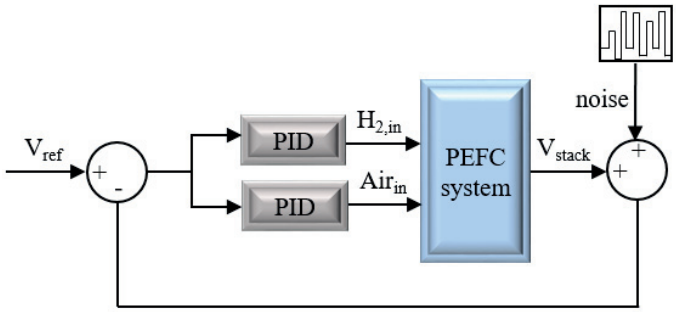

Figure 2.5: PID control scheme.

where $\dot{E}_{nernst}$ is a differentiation of equation 2.2 during one prediction horizon:

$$\dot{E}_{nernst} = k_1 \frac{1}{P_{H_2}} \dot{P}_{H_2} + \frac{k_1}{2} \frac{1}{P_{O_2}} \dot{P}_{O_2} \tag{2.47}$$

$$k_1 = 4.3085 \times 10^{-5} \times T_{stack} \tag{2.48}$$

Combining equations 2.12 - 2.15 and 2.20-2.24 $\dot{P}_{H_2}$, $\dot{P}_{O_2}$, and $\dot{P}_{N_2}$ are expressed as:

$$\dot{P}_{H_2} = \frac{k_2}{0.005} \left[k_3 m_{H_{2,in}} - k_a P_{H_2} + k_a - \frac{n_{cell} I}{2 \times F} \right] \tag{2.49}$$

$$\dot{P}_{O_2} = \frac{k_2}{0.01} \left[k_4 m_{air,in} - \frac{k_c m_{O_2}}{m_{O_2} + m_{N_2}} P_{N_2} + \frac{k_c m_{O_2}}{m_{O_2} + m_{N_2}} - \frac{n_{cell} I}{4 \times F} \right] \tag{2.50}$$

$$\dot{P}_{N_2} = \frac{k_2}{0.01} \left[k_5 m_{air,in} - \frac{k_c m_{N_2}}{m_{O_2} + m_{N_2}} P_{O_2} - \frac{k_c m_{N_2}}{m_{O_2} + m_{N_2}} P_{N_2} + \frac{k_c m_{N_2}}{m_{O_2} + m_{N_2}} \right] \tag{2.51}$$

$$k_2 = R \times T \tag{2.52}$$

$$k_3 = \frac{\rho_{H_2}}{M_{H_2} \times 60} \tag{2.53}$$

$$k_4 = 0.21 \times \frac{\rho_{O_2}}{M_{O_2} \times 60} \tag{2.54}$$

$$k_5 = 0.79 \times \frac{\rho_{N_2}}{M_{N_2} \times 60} \tag{2.55}$$

The derivative $\dot{V}_{ohmic}$ is simplified as:

$$\dot{V}_{ohmic} = I \times \dot{R}_m = 0 \tag{2.56}$$

assuming $\dot{R}_m$ is constant during the prediction horizon. The linearized continuous-time state-space model is written as:

$$\begin{aligned} \dot{\boldsymbol{x}} &= \boldsymbol{A}\boldsymbol{x} + \boldsymbol{B}\boldsymbol{u} \\ \boldsymbol{y} &= \boldsymbol{C}\boldsymbol{x} \end{aligned} \tag{2.57}$$

where the state vector $\boldsymbol{x}$ is:

$$\boldsymbol{x} = \begin{bmatrix} V_{FC} \\ V_a \\ P_{H_2} \\ P_{O_2} \\ P_{N_2} \\ 1 \end{bmatrix} \tag{2.58}$$

the input $\boldsymbol{u}$ is:

$$\boldsymbol{u} = \begin{bmatrix} m_{H_{2,in}} \\ m_{air,in} \end{bmatrix} \tag{2.59}$$

and the output $\boldsymbol{y}$ is:

$$\boldsymbol{y} = \begin{bmatrix} V_{FC} \end{bmatrix} \tag{2.60}$$

The state-space matrices are:

$$\boldsymbol{A} = \begin{bmatrix} 0 & \frac{n_{cell}}{2R_d} & A_{13} & A_{14} & A_{15} & A_{16} \\ 0 & -\frac{1}{2R_d} & 0 & 0 & 0 & \frac{I}{2} \\ 0 & 0 & \frac{-k_a k_2}{0.005} & 0 & 0 & \frac{k_2}{0.005}(k_a - \frac{n_{cell} I}{2\times F}) \\ 0 & 0 & 0 & \frac{k_2}{0.01}(-\frac{k_c m_{O_2}}{m_{O_2}+m_{N_2}}) & \frac{k_2}{0.01}(-\frac{k_c m_{O_2}}{m_{O_2}+m_{N_2}}) & \frac{k_2}{0.01}(\frac{k_c m_{O_2}}{m_{O_2}+m_{N_2}} - \frac{n_{cell} I}{4\times F}) \\ 0 & 0 & 0 & \frac{k_2}{0.01}(-\frac{k_c m_{N_2}}{m_{O_2}+m_{N_2}}) & \frac{k_2}{0.01}(-\frac{k_c m_{N_2}}{m_{O_2}+m_{N_2}}) & \frac{k_2}{0.01}(\frac{k_c m_{N_2}}{m_{O_2}+m_{N_2}}) \\ 0 & 0 & 0 & 0 & 0 & 0 \end{bmatrix} \tag{2.61}$$

$$\boldsymbol{B} = \begin{bmatrix} \frac{n_{cell} k_1 k_2 k_3}{0.005 P_{H_2}} & \frac{k_1 k_2 k_4}{0.002 P_{O_2}}) \\ 0 & 0 \\ \frac{k_2 k_3}{0.005} & 0 \\ 0 & \frac{k_2 k_4}{0.01} \\ 0 & \frac{k_2 k_5}{0.01} \\ 0 & 0 \end{bmatrix} \tag{2.62}$$

$$\boldsymbol{C} = \begin{bmatrix} 1 & 0 & 0 & 0 & 0 & 0 \end{bmatrix} \tag{2.63}$$

here

$$A_{13} = \frac{n_{cell} k_1}{P_{H_2}} \times \frac{-k_a k_2}{0.005} \tag{2.64}$$

$$A_{14} = A_{15} = \frac{n_{cell} k_1}{2 P_{O_2}} \times \frac{k_2}{0.01}(-\frac{k_c m_{O_2}}{m_{O_2} + m_{N_2}}) \tag{2.65}$$

$$A_{16} = \frac{n_{cell} k_1 k_2}{0.005 P_{H_2}}(k_a - \frac{n_{cell} I}{2 \times F}) + \frac{n_{cell} k_1 k_2}{0.02 P_{O_2}}(\frac{k_c m_{O_2}}{m_{O_2} + m_{N_2}} - \frac{n_{cell} I}{4 \times F}) - \frac{n_{cell} I}{2} \tag{2.66}$$

A quadratic programming (QP) problem will be solved at each time step to obtain the optimal control inputs:

$$\min_{\boldsymbol{u}^k} \boldsymbol{J}(\boldsymbol{u}^k) = \sum_{k=1}^{H_p} \left\| \boldsymbol{y}^k - \boldsymbol{r} \right\|_{\boldsymbol{Q}}^2 + \sum_{k=0}^{H_u-1} \left\| \boldsymbol{u}^k \right\|_{\boldsymbol{R}}^2 \tag{2.67}$$

subject to:

$$\begin{aligned} \boldsymbol{x}^{k+1} &= \boldsymbol{A^d}\boldsymbol{x}^k + \boldsymbol{B^d}\boldsymbol{u}^k \\ \boldsymbol{y}^k &= \boldsymbol{C^d}\boldsymbol{x}^k \\ \boldsymbol{u}_{lb} &\leq \boldsymbol{u}^k \leq \boldsymbol{u}_{ub} \\ \boldsymbol{x}_{lb} &\leq \boldsymbol{x}^k \leq \boldsymbol{x}_{ub} \\ \boldsymbol{x}^0 &= \boldsymbol{x}_{init} \\ k &= 0, 1, \ldots, H_p \end{aligned} \tag{2.68}$$

where $\boldsymbol{A^d}$, $\boldsymbol{B^d}$, and $\boldsymbol{C^d}$ are state-space matrices in discrete-time; H_p and H_u are prediction and control horizon length; $\boldsymbol{r}$ is the control reference; $\boldsymbol{Q}$ and $\boldsymbol{R}$ are weight tuning parameters for reference tracking and control inputs; $\boldsymbol{u}_{lb}$, $\boldsymbol{u}_{ub}$, $\boldsymbol{x}_{lb}$, and $\boldsymbol{x}_{ub}$ are the lower bounds and upper bounds of inputs $\boldsymbol{u}$ and states $\boldsymbol{x}$; and $\boldsymbol{x}_{init}$ is the latest measured value, the state feedback.

2.3 Methanol Steam Reformer Model Development

2.3.1 Hydrogen selective membrane reactor structure

Methanol steam reforming (MSR) is regarded as a promising technology to produce hydrogen for on-board fuel cell applications. The reforming catalysts largely determine the methanol conversion rate and the production of reformate gases. A great deal of research has been done to propose new catalysts with better performance for MSR. Copper-based catalysts are the most commonly used reforming catalysts for MSR because of their high catalytic activity and selectivity. Palladium-based catalysts also attract much attention due to their high stability and similar selectivity to copper-based catalysts [84]. A $Cu/ZnO/Al_2O_3$ catalyst is used in the present work for methanol steam reforming due to its high activity at low operating temperature between 250 °C and 300 °C, and high hydrogen selectivity in the reformate process [85]. The whole MSR process contains three reactions of steam reforming of methanol (SRM), methanol decomposition (MD), and water gas shift reaction (WGS) which occur in parallel. The reactions can

be summarized in R1-R3. [86].

$$CH_3OH + H_2O \leftrightarrow CO_2 + 3\,H_2, \qquad \Delta H_{jT_0} = +49.24, \quad (SRM) \qquad R_1$$
$$CH_3OH \leftrightarrow CO + 2\,H_2, \qquad \Delta H_{jT_0} = +90.41, \quad (MD) \qquad R_2$$
$$CO + H_2O \leftrightarrow CO_2 + H_2, \qquad \Delta H_{jT_0} = -41.17, \quad (WGS) \qquad R_3$$

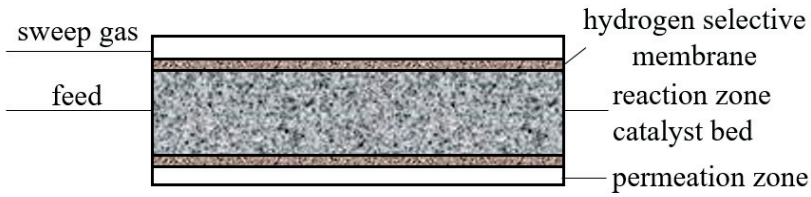

Figure 2.6: Hydrogne selective membrane reactor schematic.

From reactions (R1)–(R3), it can be seen that carbon dioxide and carbon monoxide are also produced in addition to hydrogen in the reforming process, which can easily reduce the quantity and quality of the desired hydrogen. In particular, the formation of carbon monoxide can poison the PEFC membrane when its concentration is above 10 ppm. Thus, extensive research has been carried out to purify the reformate hydrogen before sending it to fuel cell systems. Hydrogen selective membrane reactors stand out for their compatible structure and immediate separation of hydrogen from other co-products [87]. The typical schematic of a hydrogen selective membrane reactor is shown in Figure 2.6. It contains two concentric tubes. The inner tube is packed with catalyst for methanol steam reforming, and the outer tube is the shell tube for hydrogen permeation through the membrane. The operation of the membrane reactor can be described in the following way. Methanol and water vapour mixed at a specific ratio are fed into the reaction tube, while at the same time, the water vapour is also used as the sweep gas flux into the shell tube at a specific flow rate. The catalyst inside the reaction zone activates the methanol steam reforming process, producing hydrogen, carbon dioxide, and carbon monoxide. As soon as the hydrogen is produced, it permeates through the hydrogen selective membrane to the permeation zone, where the sweep gas sweeps out the permeated hydrogen gas. The permeation rate depends significantly on the hydrogen selective membrane [88]. Various studies have centred on finding efficient hydrogen selective membranes to separate hydrogen from gas mixtures to achieve high purity levels. Of these, pure Pd and its various alloys have the innate ability to allow hydrogen to selectively permeate through their structure.

In this work, a Pd/Ag membrane is adopted for its infinite permeation selectivity for hydrogen [51, 89].

2.3.2 Governing equations

According to the dissociation-solution diffusion transport mechanism, the Arrhenius law, Sievert's law, and considering the negative effects on the hydrogen permeation from other coexisting gases, the permeated hydrogen flux J_{H_2} (mol/(m^2 s)) can be derived as [88]:

$$J_{H_2} = \beta_c \frac{P_{MH_2,0}}{\delta} \times e^{-E_a/RT}[p_{tH_2}^{0.5} - p_{sH_2}^{0.5}] \tag{2.69}$$

$$\begin{aligned}\beta_c = (1 + \sqrt{K_8 p_{tH_2}})/(1 + \sqrt{K_8 p_{tH_2}} + (K_9 p_{tH_2O}) + (K_{10} p_{tCO})^{1/3} \\ + (K_{11} p_{tCO_2})^{1/2} + (K_{12} p_{tCH_3OH})^{1/2} + \frac{K_{13} K_{12} p_{tCH_3OH}}{\sqrt{K_8 p_{tH_2}}} \\ + \frac{K_{13} K_{14} K_{12} p_{tCH_3OH}}{K_8 p_{tH_2}})\end{aligned} \tag{2.70}$$

where β_c is a correction factor to account for the effects of other coexisting gases on the H_2 permeation. $P_{MH_2,0}$, δ, T, E_a, K_{8-14}, p_{tH_2}, p_{tH_2O}, p_{tCO}, p_{tCO_2}, p_{tCH_3OH} and p_{sH_2} are the pre-exponential factor (10^{-5} mol/(m s kPa$^{0.5}$)), membrane thickness (μm), reactor temperature (K), activation energy (J/mol), hydrogen permeation parameters (1/Pa), hydrogen partial pressure in the tube side (bar), water vapour partial pressure in the tube side (bar), carbon monoxide partial pressure in the tube side (bar), carbon dioxide partial pressure in the tube side (bar), methanol partial pressure in the tube side (bar) and hydrogen partial pressure in shell side (bar), respectively.

The one-dimensional steady state mathematical model developed in [88] is used in this work for the membrane reactor in Figure 2.6. The following assumptions are made. There is plug flow in the axial direction in both reaction and permeation zones; both axial and radial dispersions are neglected; radial variations in temperature and concentration are not considered; the temperature and concentration gradients in the catalyst particle are neglected; isobaric conditions are considered; and the reaction is carried out isothermally in the reactor. The major changes made in the present work from the previous study [88] can be summarized as follows: a novel Pd-Ag membrane is employed, the length of the reactor is extended and the operating pressure is increased. The molar flow rate of each component in the tube and shell side can be respectively expressed as:

$$\frac{dF_{ti}}{dz} = \pi R_1^2 \rho_B \sum_{j=1}^{M} \eta_j (\pm \nu_{ij} \gamma_j) - 2\pi R_1 J_i \tag{2.71}$$

$$\frac{dF_{si}}{dz} = 2\pi R_2 J_i \tag{2.72}$$

where F_{ti} is the molar flow rate for each component i in the tube side (mol/s), i represents the component CH_3OH, H_2O, CO_2, CO and H_2, respectively. R_1, ρ_B, η_j, ν_{ij} and γ_j are reaction tube radius (m), reforming catalyst density (kg/m^3), effectiveness factor, stoichiometric coefficient and jth reaction rate ($mol/(kg_{cat}s)$), respectively. j represents reactions R_1, R_2 and R_3. Since only hydrogen permeated to the shell side through the hydrogen selective membrane, thus, in equation 2.72 i only refers to H_2. F_{sH_2} is the molar flow rate of the hydrogen in the shell side (mol/s), J_{H_2} is the H_2 permeation flux ($mol/(m^2\ s)$), and R_2 is the shell tube radius (m). The reaction rate for reactions R_1, R_2 and R_3 can be respectively expressed as [88]:

$$r_1 = \frac{k_1 K_1 (p_{tCH_3OH} - (p_{tH_2}^3 p_{tCO_2} / K_{R_1,T} p_{tH_2O})) C_{S1} C_{S1a} S_g}{(p_{tH_2}^{0.5} + K_1 p_{tCH_3OH} + K_2 p_{tCO_2} p_{tH_2} + K_3 p_{tH_2O})(1 + K_4^{0.5} p_{tH_2}^{0.5})} \tag{2.73}$$

$$r_2 = \frac{k_2 K_5 (p_{tCH_3OH} - (p_{tH_2}^2 p_{tCO} / K_{R_2,T})) C_{S2} C_{S2a} S_g}{(p_{tH_2}^{0.5} + K_5 p_{tCH_3OH} + K_6 p_{tH_2O})(1 + K_7^{0.5} p_{tH_2}^{0.5})} \tag{2.74}$$

$$r_3 = \frac{k_3 K_1 p_{tH_2}^{0.5} (p_{tCO} p_{tH_2O} - (p_{tH_2} p_{tCO_2} / K_{R_3,T})) C_{S1}^2 S_g}{(p_{tH_2}^{0.5} + K_1 p_{tCH_3OH} + K_2 p_{tCO_2} p_{tH_2} + K_3 p_{tH_2O})^2} \tag{2.75}$$

where k_{1-3} is the kinetic constant, K_{1-7} is hydrogen permeation parameter (1/Pa), S_g is the surface area of reforming catalyst (m^2/kg), and C_S denote the total surface concentration of specific site (mol/m^2).

The following definitions are also made to evaluate the membrane reactor's performance:

CH_3OH conversion rate:

$$\frac{F_{tCH_3OH,0} - F_{tCH_3OH,out}}{F_{tCH_3OH,0}} \times 100\% \tag{2.76}$$

H_2 yield:

$$\frac{F_{tH_2} + F_{sH_2}}{F_{tCH_3OH,0}} \tag{2.77}$$

H_2 recovery:

$$\frac{F_{sH_2}}{F_{sH_2} + F_{tH_2}} \times 100\% \tag{2.78}$$

2.4 Backpropagation Neural Network Algorithm

2.4.1 Brief introduction of BP algorithm

The operating parameters of the membrane reactor can greatly affect its hydrogen production, thus causing variations in the PEFC system's performance. A simple but accurate model that can predict the system behaviour between the membrane reactor's operating parameters and the PEFC system output performance is essential for production guidance in practical and control algorithm implementation. However, it can be seen from Section 2.3.2 and Section 2.1.2 that both the membrane reactor and fuel cell models involve extensive complicated mathematical equations, making it hard to predict the system performance. Neural network algorithms are powerful tools that can be used to analyse and build the mapping relations between the input variables and output variables with the advantages of self-learning and self-adaptive ability, nonlinear mapping ability, and high fault tolerance rate [52]. The map between input and output parameters is created by providing the network with sufficient examples of input and output parameters in different conditions and then varying the network parameters to match the output to input sufficiently well. The process of varying network parameters is called training. The BP neural network algorithm is one of the most widely applied network models because of its good generalization ability and simple structure. The BP neural network algorithm is one of the most widely applied network models for its good generalization ability and simple structure [90].

2.4.2 Data collection principle of BP algorithm

The training of the backpropagation neural network requires sufficient processing examples which contain groups of matched input and output patterns [91]. Among the membrane reactor's operating conditions, the methanol feed flow rate and the steam to methanol molar ratio in the feed may strongly affect the hydrogen production and are rather easy to control during operation. The current load also has a significant effect on the PEFC system performance. Thus, in the present work, the input variables are the membrane reactor's operating parameters (steam to methanol feed ratio, S/M, the inlet flow rate of methanol, $F_{tCH_3OH,0}$) and current load of the PEFC system, I. The PEFC's voltage V_{FC} is adopted as the output variable.

Chapter 3

Analysis of Modelling and Controlling Results

In this chapter, the PEFC system model validation, control algorithm effectiveness, membrane reactor performance, and the BP neural network method prediction results are discussed.

3.1 PEFC System Model Simulation Results

This section first presents the PEFC system dynamic behaviour. Then three different PEFC systems are used to validate the PEFC system model developed in Chapter 2.

3.1.1 PEFC dynamic performance

For the dynamic performance analysis, all parameters set for the fuel cell system are extracted based on the Ballard Mark V fuel cell system and listed in Table 3.1. Notice that the variable C_{H_2} used to calculate ξ_2 in Table 3.1 is the hydrogen concentration at the anode/membrane interface (mol/cm^3), which can be expressed in equation 3.1 [57]. Figure 3.1 is the schematic of the PEFC system model, which shows that the PEFC system consists of an anode submodel, a cathode submodel, a stack temperature submodel and an output voltage submodel. Figure 3.1 also provides an overview of how the submodels are connected and coupled with each other.

$$C_{H_2} = \frac{P_{H_2}}{1.09 * 10^6 * e(\frac{77}{T_{stack}})} \tag{3.1}$$

Table 3.1: Parameters used for the PEFC system model [16, 63].

Parameter	**Value**
n_{cell}	35
ξ_1	-0.948
ξ_2	0.00286+0.0002ln$A$+(4.3e-5)lnC_{H_2}
ξ_3	7.6e-5
ξ_4	-1.93e-4
R_C (Ω)	3e-4
λ	23
β (V)	0.016
l (μm)	178
A (cm^2)	232
J_{max} (A/cm^2)	1.5
C (F)	3
F (C/mol)	96485
M_{H_2} (g/mol)	2
M_{O_2} (g/mol)	32
$k_{up,an}$ (kg/(s atm))	3.6e-5
$k_{up,ca}$ (kg/(s atm))	3.6e-4
$P_{s,an}$ (atm)	2.4
$P_{s,ca}$ (atm)	2.4
P_{atm} (atm)	1
$k_{down,an}$ (kg/(s atm))	2.2e-4
$k_{down,ca}$ (kg/(s atm))	2.2e-3
$k_{conv,amb}$ (W/K)	17
$m_{body}c_{p,body}$ (J/K)	3.5e4
$\Delta H_{R,T}$ (J/kg)	1.196e8
T_{amb} (K)	296.5

The PEFC system dynamic performance is shown in Figures 3.2-3.5. Figure 3.2 shows the current load profile consisting of two step changes. The current maintains a value of 15 A for the first 16,000 s (4.44 h), then jumps to 55 A, where it remains until 32,000 s (8.89 h). Finally, it decreases to 30 A and remains at this value until the end of the simulation at 50,000 s (13.9 h). The output voltage profile is presented in Figure 3.3. The voltage is 28.5 V when the current is 15 A, then decreases to 25.7 V after the current increases to 55 A. Finally the voltage increases to 27.0 V when the current is kept at 30 A. The varying output voltage is the result of the combination effects of the capacitance, time-varying cell body temperature, and partial pressures of hydrogen and oxygen.

Figure 3.4 shows the hydrogen and oxygen partial pressures at the anode and cathode, respectively. It can be seen that during the second 16,000 s (16,000–32,000 s) when the current is 55 A, both the hydrogen and oxygen partial pressures are lower than in the first (0–16,000 s) and third (32,000–50,000 s) stages when the

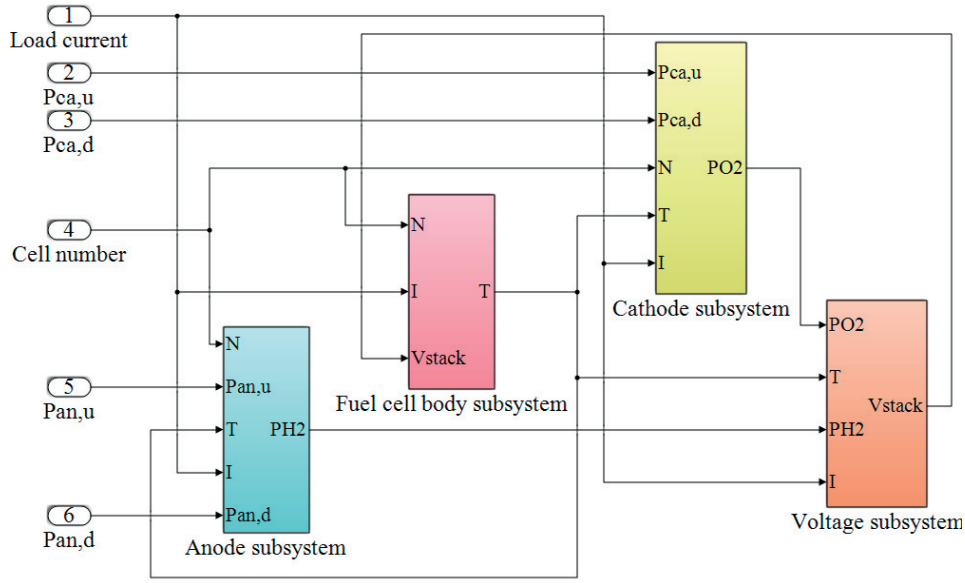

Figure 3.1: Schematic of the PEFC system model.

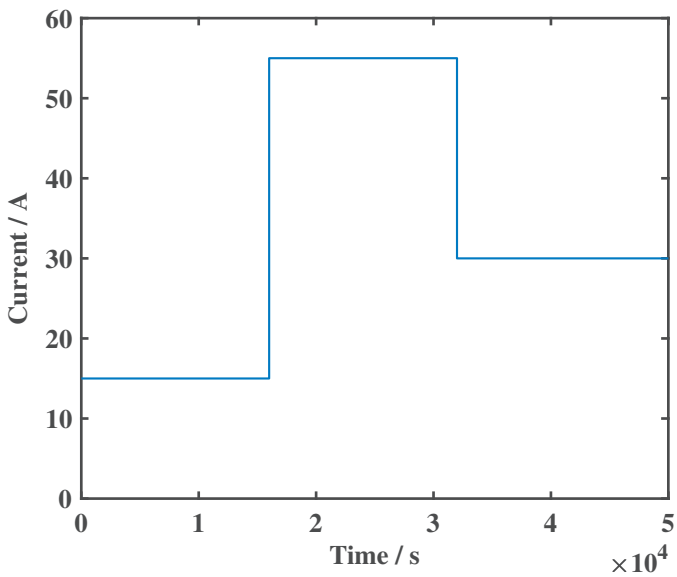

Figure 3.2: Current profile.

current is 15 and 30 A, respectively. This is because when the current is higher, the electrochemical reaction consumes more fuel and oxygen, so the reactant gas

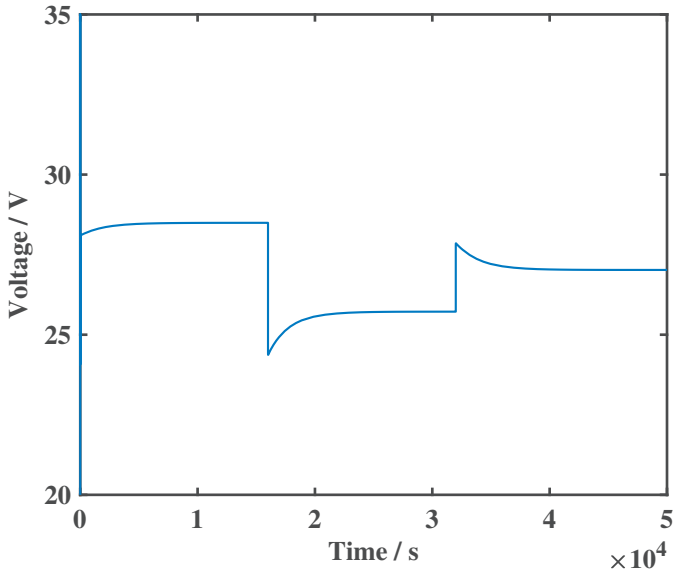

Figure 3.3: Voltage profile.

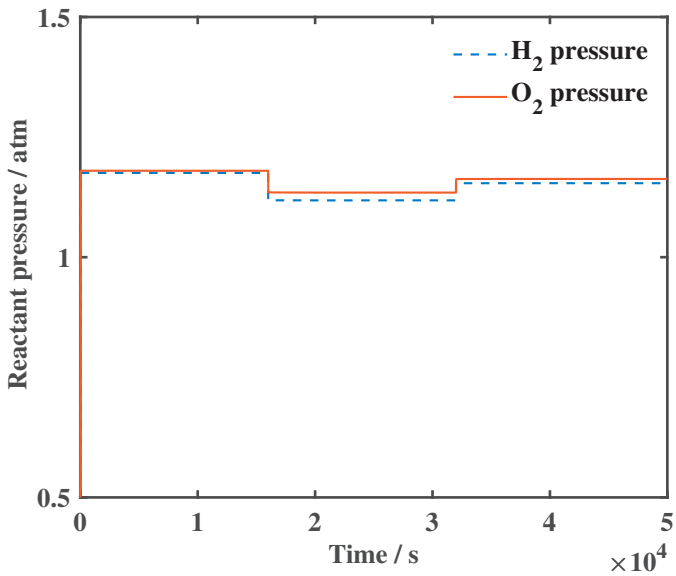

Figure 3.4: Reactant pressure profile.

pressure decreases. While the current is lower, less fuel and oxygen are consumed,

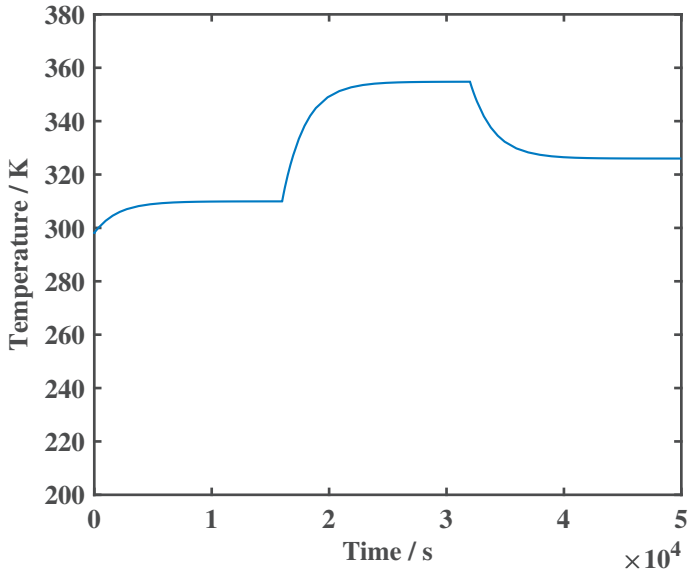

Figure 3.5: Temperature profile.

which makes the reactant pressure increase in the channel.

Figure 3.5 presents the temperature profile for the PEFC system. The temperature gradually increases to 309.9 K from room temperature during the first 16,000 s due to the heat generated by the electrochemical reaction. Then it keeps increasing until it reaches 354.7 K during the second stage (16,000–32,000 s) when the current is at 55 A. Finally, the temperature slowly drops to 326.0 K when the current load is decreased to 30 A. It is worth noting that under each load change, the investigation of faster processes like reactant pressure requires less simulation time to generate the complete stable response. However, there is always a large response delay in the temperature profile under load changes. The response delay in the temperature profile is because the thermal variations within the stack usually require more time (1800–6,000 S) to reach a steady state. Similar results were obtained in [16, 92], where their developed models take 50–83 min for the temperature and voltage to reach steady state for each load change.

3.1.2 Ballard Mark V PEFC system model validation

In this section, the Ballard Mark V fuel cell system [93] is employed to validate the PEFC system model concerning the application for the start-up, power

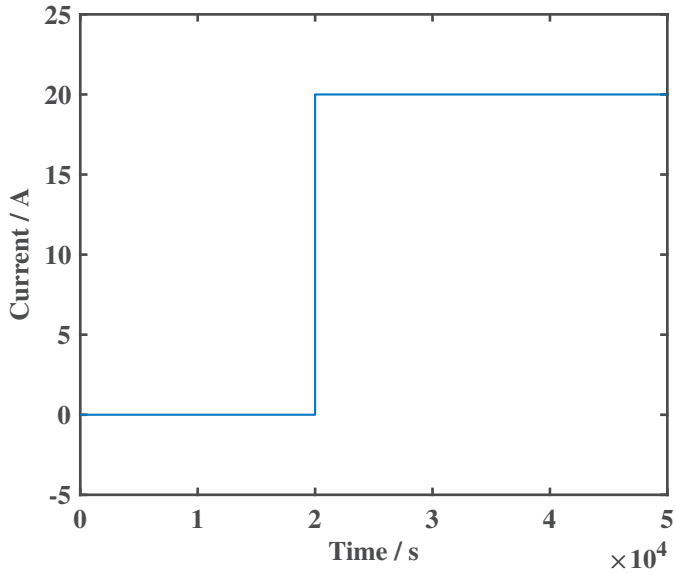

Figure 3.6: Current change in start-up.

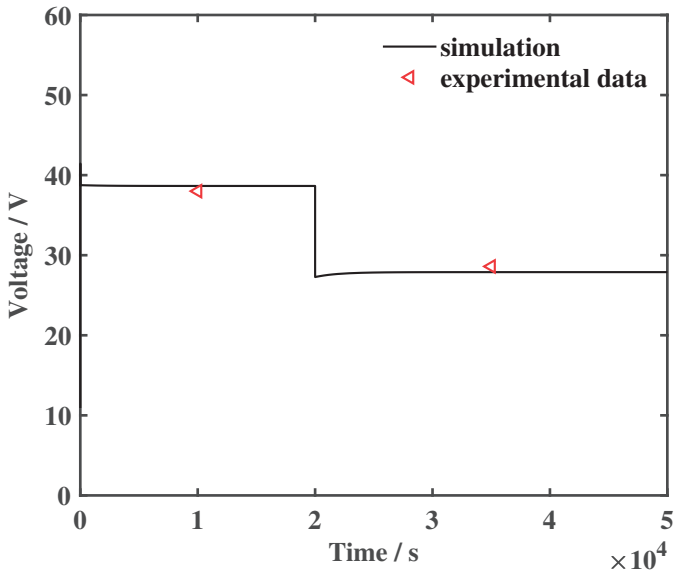

Figure 3.7: Voltage response in start-up.

step up and shut down of the PEFC system. The parameters needed are listed

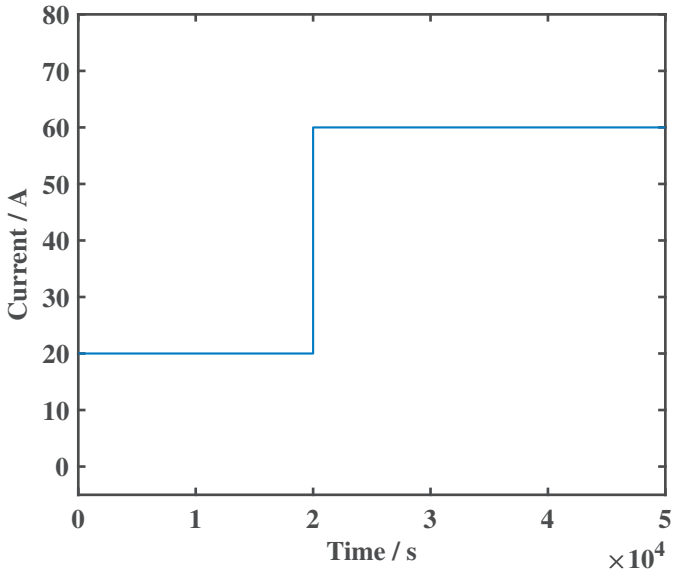

Figure 3.8: Current change in power step up.

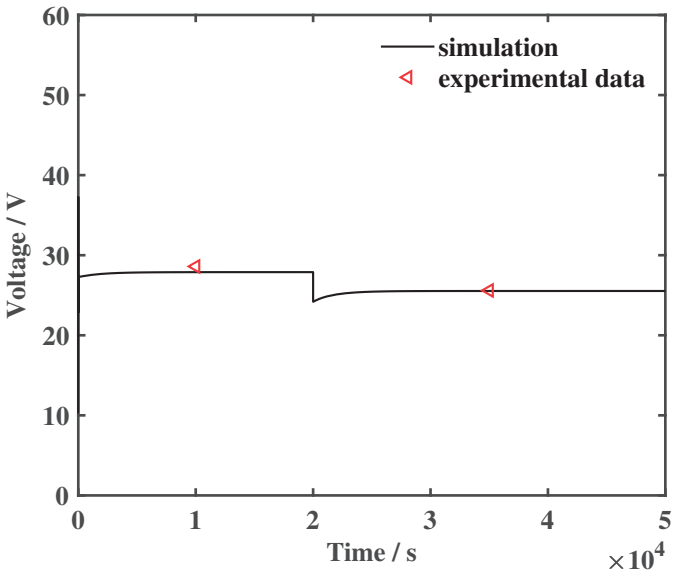

Figure 3.9: Voltage response in power step up.

in Table 3.1. To clarify, the experimental data extracted from [93] are steady

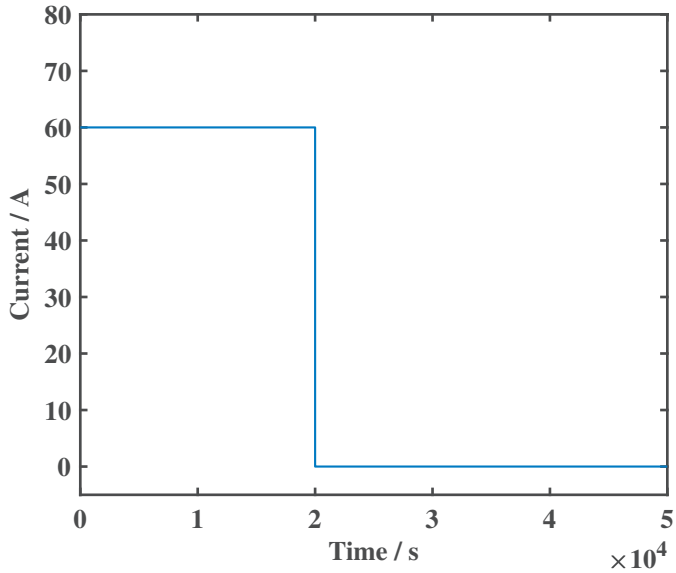

Figure 3.10: Current change in shut down.

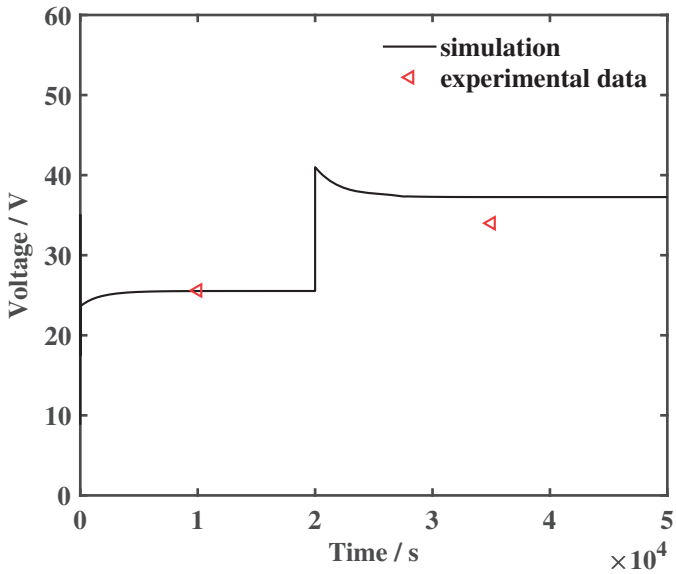

Figure 3.11: Voltage response in shut down.

state data and they are compared with the steady state results from our PEFC

system dynamic model. During the tests, the current load is set as the input signal with the voltage as the output testing response. Figure 3.6 shows the step change of the current for the start-up from 0 to 20 A. Figure 3.7 compares the experimental and simulated output voltages. The results show that the experimental voltage response changes from 38.0 V to 28.6 V and the simulated voltage changes from 38.3 V to 28.3 V, which is a good agreement between simulation and experiment. Figure 3.8 shows the power step up of the PEFC system when current steps from 20 A to 60 A. It can be seen from Figure 3.9 that the corresponding experimental output voltage changes from 28.6 V to 25.6 V and the simulated voltage response changes from 28.3 V to 25.6 V. Again, good agreement between the model prediction and experimental results are achieved. Figure 3.10 exhibits the current change for the shut-down of the PEFC system from 60 A to 0 A. Figure 3.11 shows the experimental voltage response changes from 25.6 V to 34.0 V and the simulated voltage changes from 25.6 V to 38.3 V. It is noticeable that the experimental data is lower than the simulated voltage response when the load current drops to 0 A, which may be attributed to the degradation of the PEFC system in practice.

3.1.3 NedSstackPS6 PEFC system model validation

In this section, the commercial stacked PEFC-NedSstackPS6 [58] is applied to validate the PEFC system model. Air is supplied at the system cathode instead of oxygen.

All parameters needed for the cell system are presented in Table 3.2. The system performance under different operating conditions is shown in Figure 3.12. Figure 3.12 (a) shows the PEFC system performance with the hydrogen flow rate varying from 100 to 400 lpm. Figure 3.12 (b) presents the PEFC system performance with the air flow rates increasing from 300 to 700 lpm. It can be clearly seen that increasing hydrogen and air flow rate both slightly improve the PEFC system voltage. Moreover, our model shows good agreement with Monem's model [94] To clarify, in Monem's model, the voltage increase under the air flow rate from 300 to 700 lpm is very small, which almost overlapped, making it difficult to capture. Thus, in Figure 1B, only one line is shown for his model.

3.1.4 Horizon 500 W PEFC system model validation

In this section, the Horizon 500 W PEFC system [58] is used to validate the PEFC system model. The Horizon 500 W PEFC model is developed based on equations 2.1-2.11. All parameters needed for the fuel cell system are listed in Table 3.3. The simulation results are presented in Figure 3.13. Figure 3.13 (a)

Table 3.2: Parameters used for PEFC-NedSstackPS6 [94].

Parameter	**Value**
n_{cell}	65
ξ_1	-1.023071
ξ_2	3.4760e-3
ξ_3	7.7883354e-5
ξ_4	-9.54e-5
R_C (Ω)	1.62e-4
λ	15.03229
β (V)	0.0136
l (μm)	178
A (cm^2)	240
J_{max} (A/cm^2)	0.918
M_{H_2} (g/mol)	2
M_{O_2} (g/mol)	32
k_a (mol/(s atm))	0.065
k_c (mol/(s atm))	0.065
T (K)	332-342
Fuel flow rate (lpm)	100-400
Air flow rate (lpm)	300-700

shows the current and temperature input conditions and Figure 3.13 (b) displays the PEFC system output voltage compared with the experimental data. The input conditions and experimental data are extracted from [95]. The current profile contains a series of step changes and along with the temperature profile is used as the input of the PEFC system model. Figure 3.13 (b) shows that good agreement is achieved between our simulation results and the experimental results, which proves the reliability of the PEFC system model.

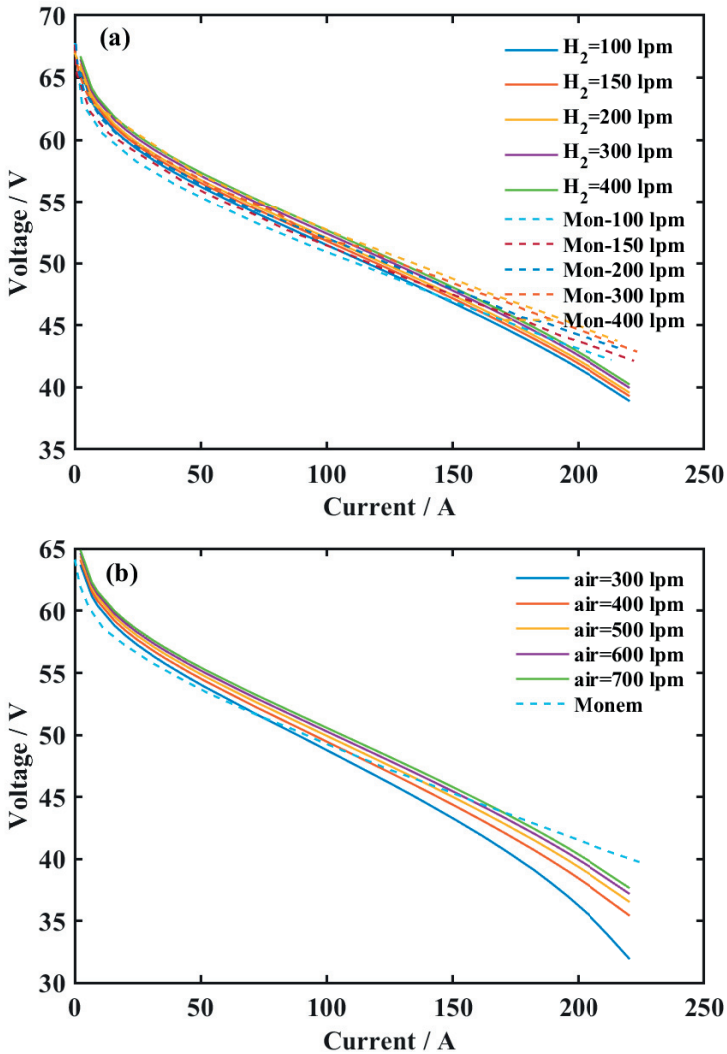

Figure 3.12: Model validation.

3.2 Controlling Simulation Results

3.2.1 PEFC system temperature control results using MPC

The cooling model and temperature control strategies are applied to the Ballard Mark V PEFC system. The effectiveness of the developed controllers are evaluated in two different operating conditions: 1) a typical perturbation in the current load, 2) random perturbation in the current load. The parameters needed are listed in Table 3.4.

Table 3.3: Parameters used for the Horizon 500 W PEFC system [58].

Parameter	**Value**
n_{cell}	36
ξ_1	-0.853200
ξ_2	2.522e(-3)
ξ_3	7.843743e(-5)
ξ_4	-16.3e(-5)
R_C (Ω)	7.999e(-4)
λ	13
β (V)	0.048869
l (μm)	25
A (cm^2)	52
J_{max} (A/cm^2)	0.51923
C (F)	2
P_{H_2} (atm)	0.55
P_{O_2} (atm)	1

Table 3.4: Parameters used for the thermal model [96].

Parameter	**Value**
ρ_{air} (kg/m^3)	1.225
$C_{p,air}$ (J/(kg K))	1004
ΔT (K)	30

Case study 1 In this case, the current load is disturbed with two typical step changes: one large increase and one large drop, as shown in Figure 3.14. The air flow rate changes are displayed in Figure 3.15. The temperature profile using MPC and PID control is presented in Figure 3.16. At 20,000 s, when the current load jumps from 10 A to 100 A, the heat generated by the electrochemical reaction jumps, which produces a significant amount of excess heat and makes the stack temperature increase rapidly. However, due to the regulation of the MPC and PID controllers, the stack temperature is perfectly maintained at 343 K by adjusting the air flow rate to a suitable value of 76.4 CFM. At 40,000 s, when the current load steps down from 100 A to 50 A, the heat generated decreases rapidly, while the stack temperature is still controlled at 343 K by the MPC and PID controllers with the air flow rate decreases to 6.27 CFM. It can be seen that both the MPC and the PID controllers are effective in stabilizing the temperature of the PEFC system. However, the MPC controller is much superior to the PID controller in tracking the desired temperature with no oscillations occurring. Its response under each load step change is much faster.

Case study 2 In this case, the current load is disturbed by random perturbations, a series of stochastic step changes as shown in Figure 3.17. The corresponding

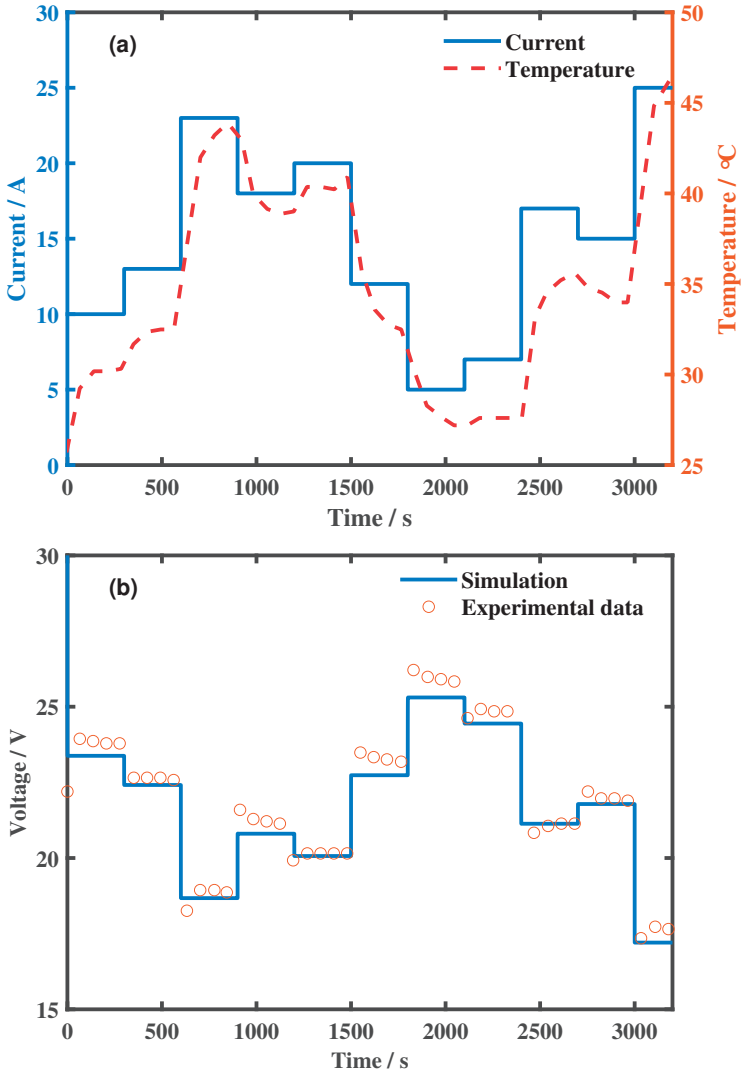

Figure 3.13: (a) Current and temperature input conditions of PEFC system; (b) PEFC system output voltage.

stack temperature profile with MPC and PID control is presented in Figure 3.18. The figure shows that for any stochastic perturbation, both MPC and PID are able to stabilize the stack temperature at 343 K. However, the MPC controller is much more effective in eliminating the system error without any oscillation and time delay for each input signal step change.

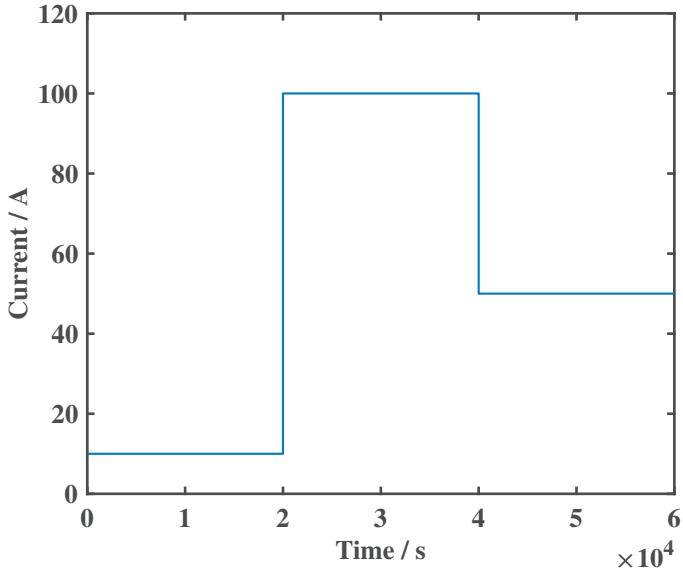

Figure 3.14: Load changes in case study 1.

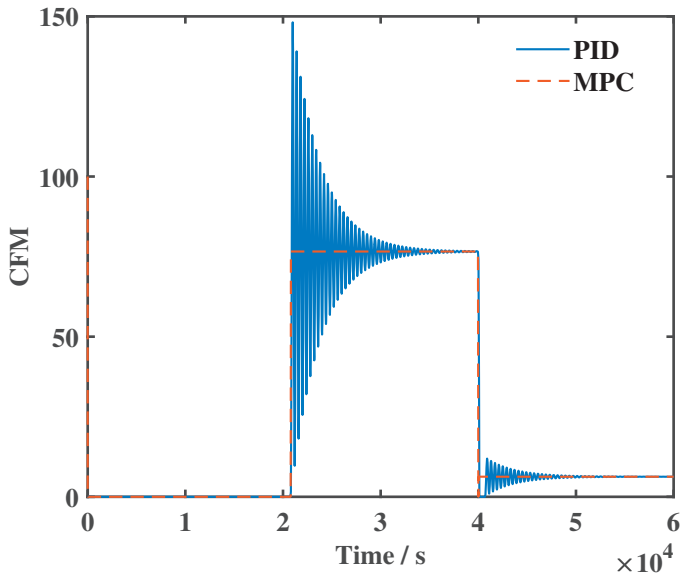

Figure 3.15: CFM changes in case study 1.

3.2.2 PEFC system voltage control results by MPC

In this section, the voltage control strategies are applied to the NedSstackPS6 PEFC system. The effectiveness of the developed controllers are investigated in

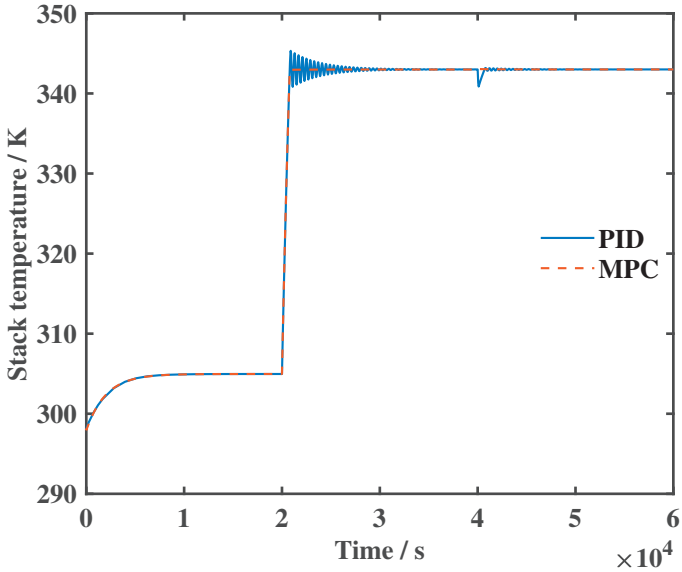

Figure 3.16: Temperature changes in case study 1.

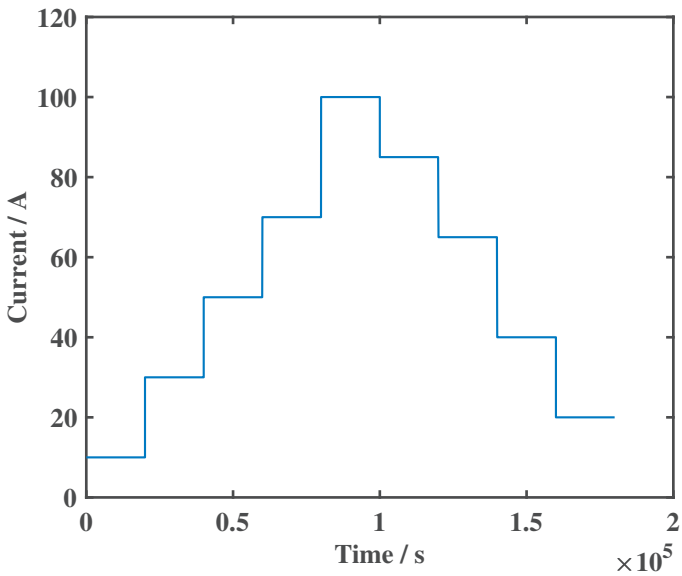

Figure 3.17: Load changes in case study 2.

two different case studies: 1) typical disturbance applied to the working load, 2)

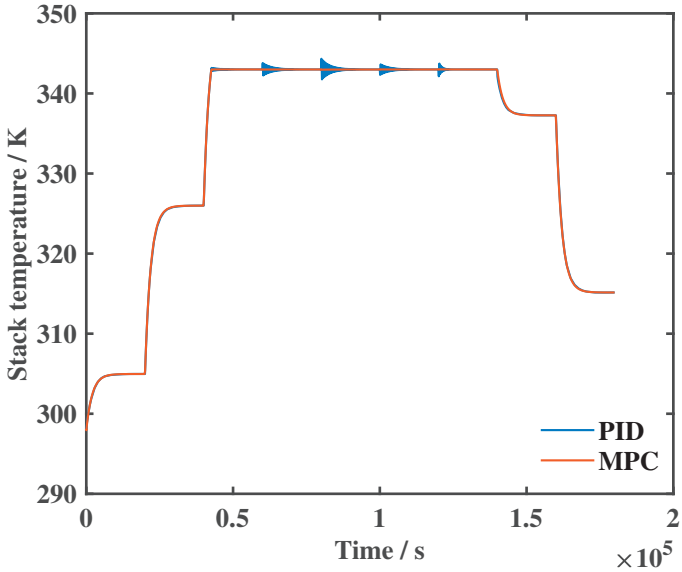

Figure 3.18: Temperature changes in case study 2.

random disturbance applied to the working load.

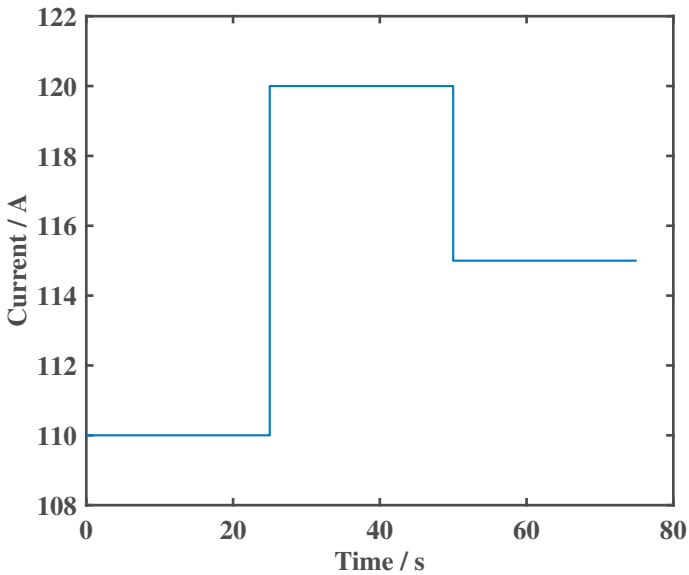

Figure 3.19: Load changes in case study 1.

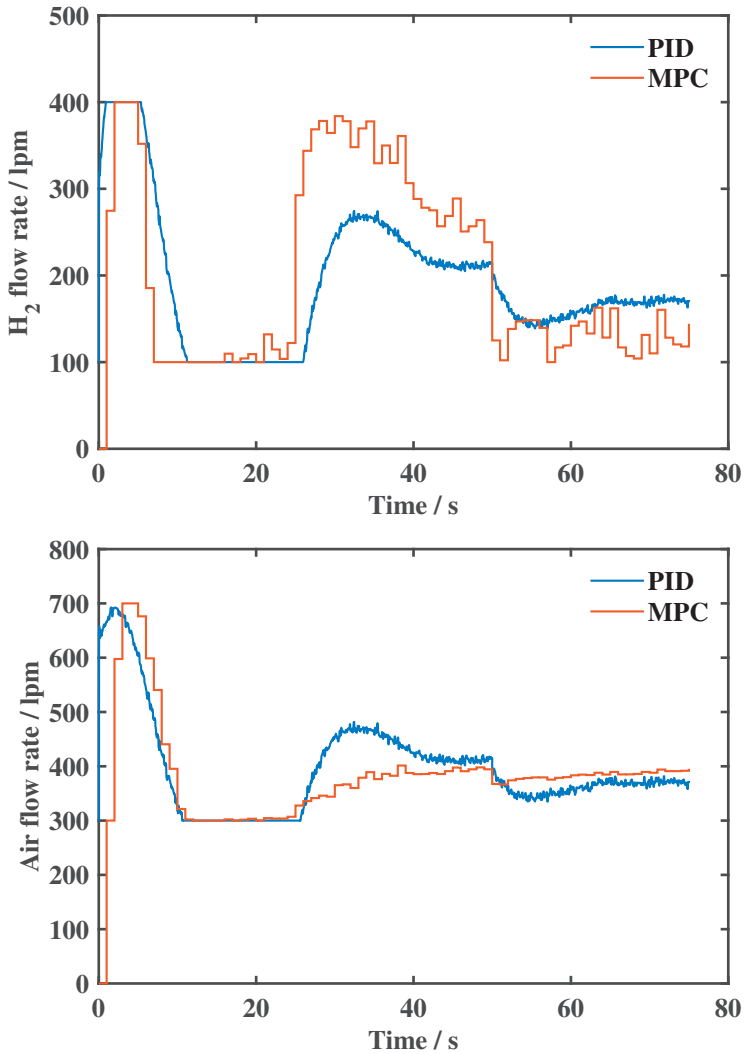

Figure 3.20: Hydrogen and air flow rate changes in case study 1.

Case study 1 In this case, the current load is interrupted by a sudden increase and a sudden decrease as shown in Figure 3.19. The hydrogen and air flow rate profiles under the control of PID and MPC controllers are shown in Figure 3.20. When the current jumps from 110 A to 120 A at 25 s, the output voltage is supposed to drop according to polarization theory. However, the controller will try to increase the hydrogen and air flow rates to a higher level, thus increasing the hydrogen and oxygen partial pressures to keep the voltage at the desired 48 V. At 50 s, when the current load drops from 120 A to 115 A, the output voltage

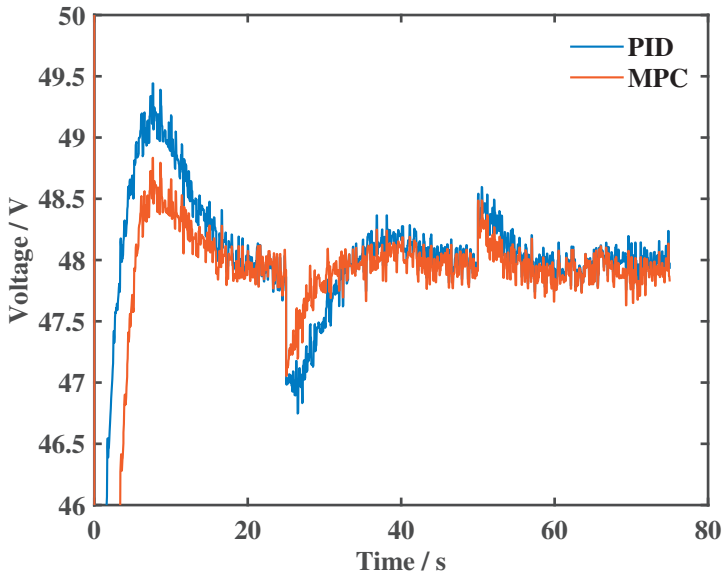

Figure 3.21: Voltage changes in case study 1.

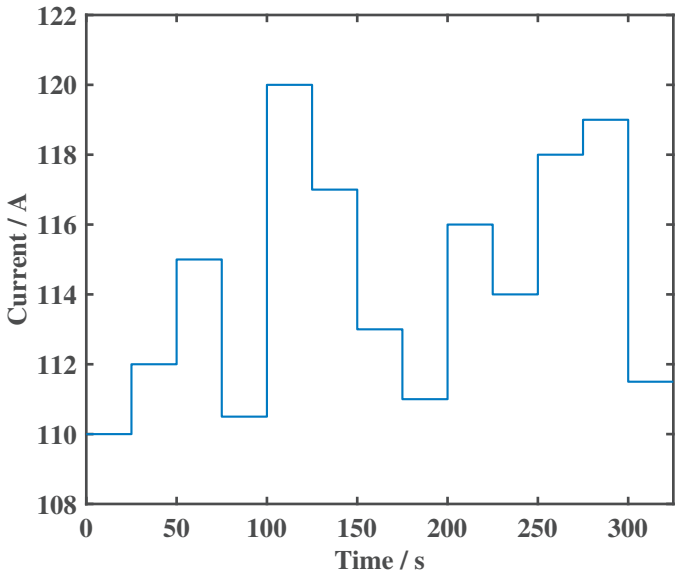

Figure 3.22: Load changes in case study 2.

is supposed to increase. The controllers then regulate the hydrogen and air flow

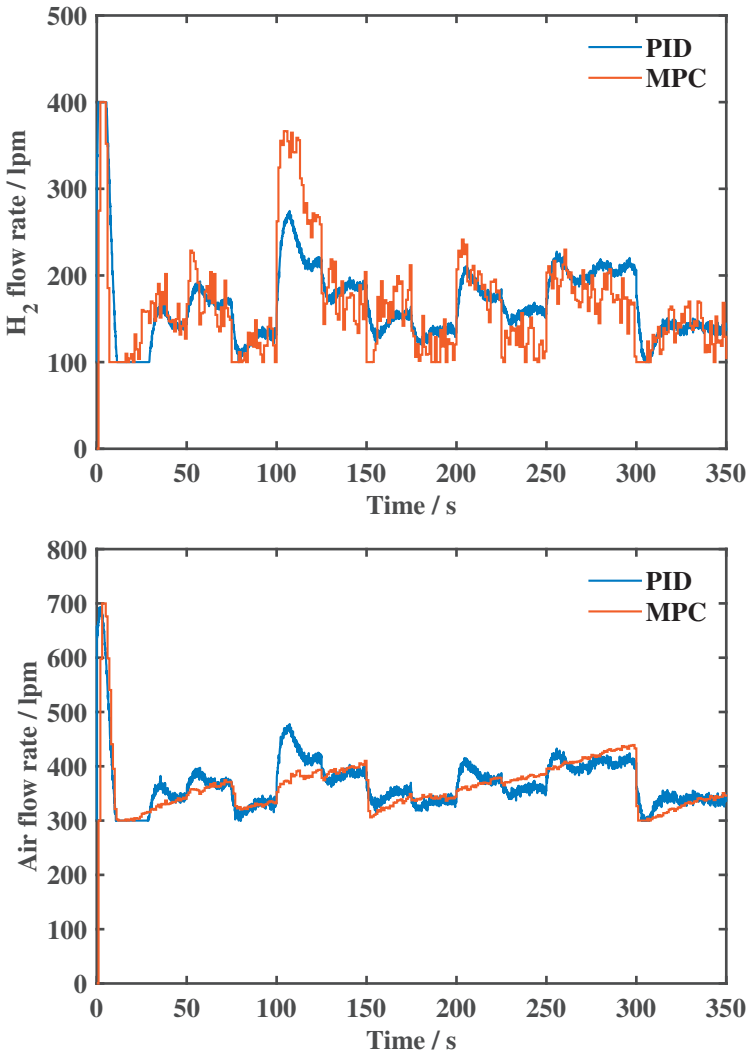

Figure 3.23: Hydrogen and air flow rate changes in case study 2.

rates to a lower level to reduce their pressure to stop the voltage increase, and thus the voltage is kept at the reference value of 48 V. The voltage profile is exhibited in Figure 3.21. Both the PID and MPC controllers can keep the PEFC system's output voltage at the desired 48 V, but clearly the MPC shows superior performance with faster response and lower oscillation.

Case study 2 In this case, the current load is disturbed by random perturbations composed of a series of stochastic step changes, as shown in Figure 3.22. Figure

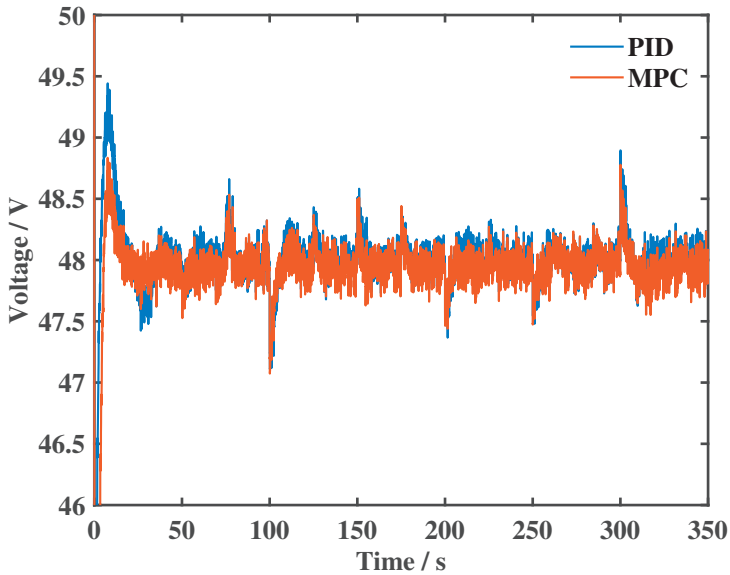

Figure 3.24: Voltage changes in case study 2.

3.23 displays the hydrogen and air flow rate profiles. The corresponding voltage profile is shown in Figure 3.24, from which it is clear that for any random disturbance, both MPC and PID are qualified to control the voltage to 48 V. However, again the MPC controller shows superior performance with smaller overshoot and faster response for each step change in the current load.

3.3 Membrane Reactor and BP Algorithm Results

In this section, the hydrogen produced from the membrane reactor is used as fuel for the Horizon 500 W PEFC system. Then the BP neural network is trained to find the hidden model between the membrane reactor operating conditions and the Horizon 500 W PEFC system output voltage.

3.3.1 Membrane reactor model simulation results

All parameters used for the membrane reactor are listed in Table 3.5. The simulation result is shown in Figure 3.25. It can be seen that the developed hydrogen selective membrane reactor model is able to produce fuel cell grade hydrogen. The outlet molar flow rate of methanol $F_{tCH_3OH,out}$, tube side hydrogen molar flow rate F_{tH_2} and shell side hydrogen molar flow rate F_{sH_2} are 1.1437 µmol/s, 0.0056 mol/s and 0.0055 mol/s, respectively. According to equations

Table 3.5: Parameters used for the membrane reactor model [88, 97].

Parameter	**Value**
k_1	$7.4e14 \times e^{(-12364.69/T)}$
k_2	$3.8e20 \times e^{(-20447.44/T)}$
k_3	$5.9e13 \times e^{(-10536.45/T)}$
K_1	$6.55e(-3) \times e^{(2405.58/T)}$
K_2	$2.3e9 \times e^{(-12027.91/T)}$
K_3	$4.74e(-3) \times e^{(2405.58/T)}$
K_4	$5.43e(-6) \times e^{(6013.95/T)}$
K_5	$36.9e^{(2405.58/T)}$
K_6	$36.9e^{(2405.58/T)}$
K_7	$3.86e(-3) \times e^{(6013.95/T)}$
K_8	$3.33e(-10) \times e^{(58462/RT)}$
K_9	$1.54e(-10) \times e^{(49114/RT)}$
K_{10}	$6.38e(-11) \times e^{(88423/RT)}$
K_{11}	$3.67e(-15) \times e^{(106217/RT)}$
K_{12}	$1.69e(-16) \times e^{(123367/RT)}$
K_{13}	$3.77e38 \times e^{(-418858/RT)}$
K_{14}	$4.44e29 \times e^{(-328792/RT)}$
C_{s1}, C_{s2} (mol/m^2)	7.5e(-6)
C_{s1a}, C_{s2a} (mol/m^2)	1.5e(-5)
S_g (m^2/kg)	1.02e5
E_a (J/mol)	14620
$P_{MH_2,0}$ [10^{-5} mol/(m s kPa$^{0.5}$)]	1.00
δ (μm)	5
$P_t(bar)$	4
$P_s(bar)$	1
T (K)	593
$F_{tCH_3OH,0}$ (mol/s)	4e-3
reactor length L (m)	0.5
η_j	1
R_1 (m)	0.005
R_2 (m)	0.005+5e(-6)
ρ_B (kg/m^3)	1300
steam to methanol feed ratio, S/M	1.5
sweep ratio, SR	4

2.76-2.78, the conversion rate of CH_3OH reaches 99%, the H_2 yield reaches 2.78 and 50% H_2 recovery is realized. It is notable that the CH_3OH conversion rate is rather high. This is because the permeation of H_2 from the tube side to the shell side through the hydrogen selective membrane enables a shift in the equilibrium of the methanol steam reforming reaction toward the production, thus leading to more conversion of the reactants. And at the start of the reaction, the hydrogen molar flow rate in the tube side increases significantly, but then

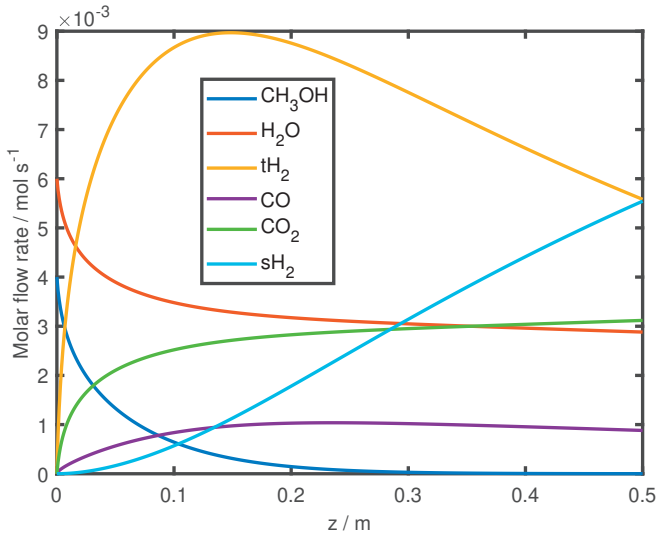

Figure 3.25: Components molar flow rates.

gradually decreases with the permeation of hydrogen to the shell side through the membrane. It is clear that the hydrogen molar flow rate at the shell side continuously increases. The hydrogen permeation also favours the R_3 reaction, reducing the concentration of CO but increasing the molar flow rate of H_2 and CO_2.

3.3.2 BP algorithm results

Raw data collection from membrane reactor and the Horizon 500 W PEFC system for BP method

The input parameters values are presented in Table 3.6, based on which a 7^3 orthogonal experiment is then designed and conducted in our model to collect raw data for training the network. The collected raw data are listed in Table 3.7 and Table 3.8.

Table 3.6: Input variables design for network training.

Inputs	1	2	3	4	5	6	7
$F_{tCH_3OH,0}$ (mol/s)	1.5e-3	2.0e-3	2.5e-3	3.0e-3	3.5e-3	4.0e-3	4.5e-3
S/M	1	1.0833	1.1667	1.25	1.3333	1.42	1.5
I (A)	5	6.6667	8.3333	10	11.6667	13.3333	15

Table 3.7: Orthogonal experiment design.

Cases	Inputs			Output
	$F_{tCH_3OH,0}$ (mol/s)	S/M	I (A)	V_{FC} (V)
1	1.5e-3	1	5	26.9148
2	1.5e-3	1.0833	6.6667	26.0975
3	1.5e-3	1.1667	8.3333	25.3639
4	1.5e-3	1.25	10	24.6578
5	1.5e-3	1.3333	11.6667	23.9548
6	1.5e-3	1.42	13.3333	23.1498
7	1.5e-3	1.5	15	22.0016
8	2.0e-3	1	6.6667	26.2419
9	2.0e-3	1.0833	8.3333	25.5338
10	2.0e-3	1.1667	10	24.8657
11	2.0e-3	1.25	11.6667	24.2256
12	2.0e-3	1.3333	13.3333	23.5472
13	2.0e-3	1.42	15	22.8230
14	2.0e-3	1.5	5	27.0368
15	2.5e-3	1	8.3333	25.6228
16	2.5e-3	1.0833	10	24.9679
17	2.5e-3	1.1667	11.6667	24.3471
18	2.5e-3	1.25	13.3333	23.6991
19	2.5e-3	1.3333	15	23.0365
20	2.5e-3	1.42	5	27.0996
21	2.5e-3	1.5	6.6667	26.3029
22	3.0e-3	1	10	25.0279
23	3.0e-3	1.0833	11.6667	24.4156
24	3.0e-3	1.1667	13.3333	23.7780
25	3.0e-3	1.25	15	23.1371

BP neural network structure

The configuration of the BP neural network algorithm is shown in Figures 3.26 and 3.27. It can be seen that three input variables ($F_{tCH_3OH,0}$, S/M, and I) are used as the input layer with each one corresponding to a neuron. The output variable V_{FC} is used as the output layer with one neuron. The input layer is connected sequentially to the output layer through two hidden layers. The connections between layers contain weights, and each layer includes a set of neurons. Each single neuron is connected to all other neurons of a previous layer through adaptable synaptic weights. The result of the training process greatly depends on the number of hidden layer neurons. To obtain the optimized results, the optimal number of hidden layer neurons should be selected. There are usually two ways of selecting the number of hidden layer neurons. One way is to use an optimized algorithm technique, and the other way is the trial and error method. In this work, the trial and error method is adopted to select the

Table 3.8: Orthogonal experiment design continued.

Cases	Inputs			Output
	$F_{tCH_3OH,0}$ (mol/s)	S/M	I (A)	V_{FC} (V)
26	3.0e-3	1.3333	5	27.1371
27	3.0e-3	1.42	6.6667	26.3434
28	3.0e-3	1.5	8.3333	25.6440
29	3.5e-3	1	11.6667	24.4593
30	3.5e-3	1.0833	13.3333	23.8298
31	3.5e-3	1.1667	15	23.1965
32	3.5e-3	1.25	5	27.1612
33	3.5e-3	1.3333	6.6667	26.3693
34	3.5e-3	1.42	8.3333	25.6715
35	3.5e-3	1.5	10	25.0189
36	4.0e-3	1	13.3333	23.8641
37	4.0e-3	1.0833	15	23.2357
38	4.0e-3	1.1667	5	27.1778
39	4.0e-3	1.25	6.6667	26.3864
40	4.0e-3	1.3333	8.3333	25.6896
41	4.0e-3	1.42	10	25.0377
42	4.0e-3	1.5	11.6667	24.4226
43	4.5e-3	1	15	23.2645
44	4.5e-3	1.0833	5	27.190
45	4.5e-3	1.1667	6.6667	26.3986
46	4.5e-3	1.25	8.3333	25.7019
47	4.5e-3	1.3333	10	25.0505
48	4.5e-3	1.42	11.6667	24.4351
49	4.5e-3	1.5	13.3333	23.7971

neuron numbers and ensure relatively good prediction performance. During the BP neural network training process, the data stream spreads forward but the error signal spreads backwards. The forward propagating direction is input layer $\longrightarrow$ hidden layers $\longrightarrow$ output layer. The state of each neuron of each layer only affects the neurons of the next layer. If the expected output cannot be achieved, the error signal is back-propagated to adjust the values of neurons between the output and the input.

From the 49 groups of training data in Table 3.7 and Table 3.8, the BP network algorithm randomly selects 40 groups as the training group and the remaining 9 groups as the validation group. The mean square error (MSE), as expressed in equation 3.2 as well as the maximum prediction deviation are used to evaluate the prediction performance of the network. In equation 3.2, n is the number of the validation group and i is the index of the group. E is the expected result, which is the modelling result here. P is the neural network prediction. The prediction deviation therefore means the difference between E and P. By using

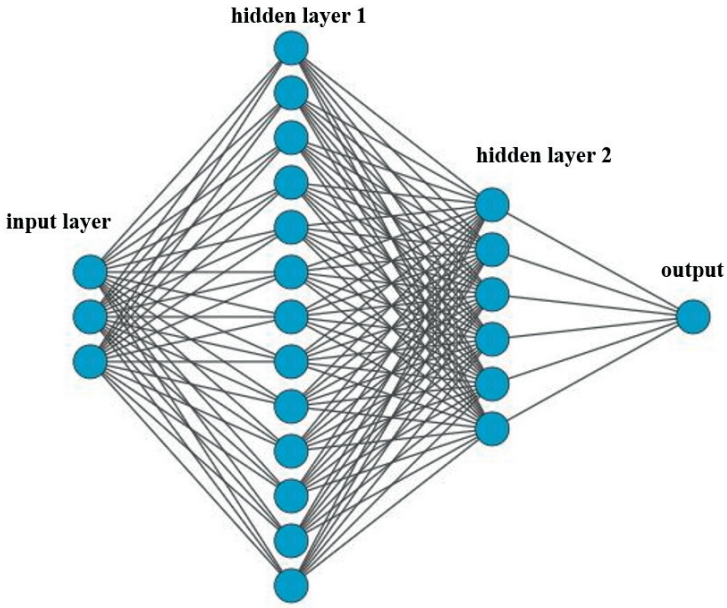

Figure 3.26: Back propagation neural network structure.

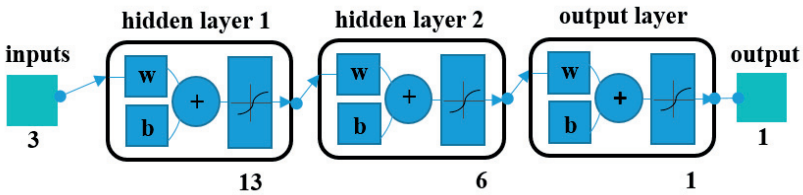

Figure 3.27: Back propagation neural network configuration.

several combinations of the neuron numbers in the two hidden layers, the MSE and the maximum prediction deviation are recorded and compared. Finally, a 3-13-6-1 network structure (Figure 3.27), is chosen for the network as the MSE and the maximum deviation are both small compared to other configurations.

$$MSE = \frac{1}{n}\sum_{i=1}^{n}(E_i - P_i)^2 \tag{3.2}$$

BP algorithm prediction results

The prediction results of the back propagation neural network are presented in Figure 3.28 and Figure 3.29. Figure 3.28 (a) shows the BP network prediction

error and Figure 3.28 (b) gives the prediction error as a percentage. It can be seen that the sample errors are controlled in a rather small range with the sum of errors as 1.2038 V and the MSE at 0.0260 V according to equation 3.2. Figure 3.29 presents the predicted output of the BP network algorithm, which shows good agreement with the expected output. Therefore, it can be concluded from the simulation results that the BP neural network can capture the characteristics of the input data and predict the outputs as expected.

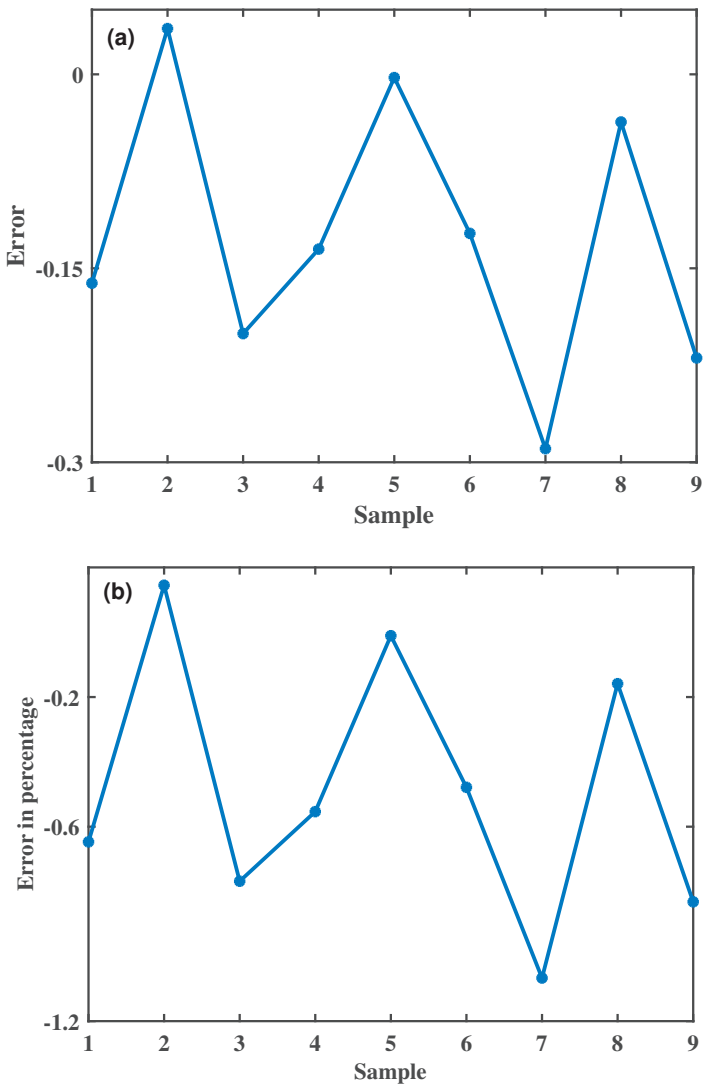

Figure 3.28: Back propagation neural network error analysis.

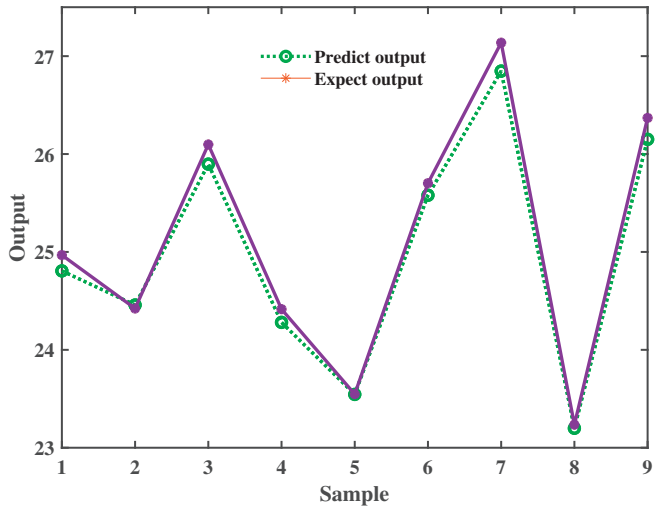

Figure 3.29: Back propagation neural network output.

Chapter 4

Conclusions and Outlook

4.1 Summary and Conclusions

This thesis is focused on the modelling and controlling of PEFC systems with different sizes of 5 kW, 6 kW and 500 W. The first part investigates the modelling methodology of a PEFC system, the controlling methodology for PEFC systems' temperature regulation and voltage control, the modelling method for membrane reactor to produce fuel cell grade hydrogen, and the neural network algorithm for system behaviour prediction. The second part presented the PEFC system's dynamic performance, controlling effectiveness, membrane reactor's modelling results, and BP algorithm's prediction performance.

The following presents the main conclusions obtained from the conducted work:

- A system level dynamic PEFC model was developed based on a set of semi-empirical equations. The cell dynamic performance such as output voltage, reactant partial pressure, and stack temperature were investigated under various load conditions. Simulation results showed that the PEFC model is qualified to characterize the PEFC's transient performance. For each load change, the output voltage and stack temperature require much time to reach the steady state. Good agreement was achieved between the simulation results and experimental data, proving the model's reliability.
- Novel MPC controllers were developed and implemented in the PEFC systems with the applications in temperature control and voltage regulation. The simulation results showed that the MPC controllers perform much better than PID controllers with much smaller oscillation and much faster response times in restraining system disturbances and tracking the reference values. The developed MPC controllers can easily be employed in PEFC systems for other control applications .

- A novel hydrogen selective membrane reactor was developed for MSR to produce fuel cell grade hydrogen for a Horizon 500 W PEFC system. The membrane reactor shows good performance with a 99% methanol conversion rate, 2.78 hydrogen yield and 50% hydrogen recovery. A BP neural network algorithm was used to build a concise mapping relation model between the membrane reactor's operating parameters and PEFC system output performance to predict the system behaviour. The mapping relation model can be used for future system integration design and control algorithm implementation.

4.2 Future Outlook

Future work will be focused on further study of PEFC system modelling and experimental work for better model validation. More effective and reliable control algorithms will be investigated and implemented to improve the PEFC system's performance. More efficient artificial network algorithms will also be studied and trained for PEFC system behaviour prediction. The following projects are recommended:

- The PEFC system's auxiliary components (e.g. air compressor, hydrogen tank radiator, inverter, and pump) should be modelled and integrated with the PEFC stack for further system behaviour study under different working conditions. The appropriate experiments should also be conducted to validate the model.

- More advanced control algorithms such as sliding mode control, nonlinear control and generalized predictive control should be studied for PEFC system applications in power consumption reduction, minimum fuel consumption tracking, stability improvement and efficiency maximization.

- Other effective artificial network algorithms like radial basis function networks and Elman neural networks can be studied to provide useful and reasonably accurate input–output relations of the PEFC system model instead of building complicated mathematical equations.

Chapter 5

Summary of Publications

Paper i: Temperature control strategy for polymer electrolyte fuel cells

Y.X. Qi, X.F. Li, S.A. Li, T.S. Li, M. Espinoza-Andaluz, P. Tunestål, M. Andersson
International Journal of Energy Research, 44.6 (2020): 4352-4365

This paper proposes two different controllers: a novel MPC controller and a novel PID controller to control the PEFC system temperature at an optimal value by regulating the coolant flow rate. The MPC controller is superior to the PID controller in restraining system disturbances and tracking the reference temperature with smaller overshoot and faster response under load changes.

The candidate organized the paper's methodology, developed the cooling model for the PEFC system, carried out the simulation, and performed the post processing and analysis of data. PhD student Xiufei Li developed the MPC and PID control algorithms. Supervisors assisted in paper writing and research planning.

Paper ii: A multi-input and single-output voltage control for a polymer electrolyte fuel cell system using model predictive control method

X.F. Li, **Y.X. Qi**, S.A. Li, P. Tunestål, M. Andersson
International Journal of Energy Research, 45.9(2021): 12854-12863

This paper studies a novel MPC controller to stabilize the PEFC system voltage by regulating its input hydrogen and air flow rates at the same time, which synthesizes a MISO control problem. The MPC controller is more robust and

superior to the PID controller in maintaining the voltage at the desired value.

The candidate organized the paper's methodology, developed and validated the PEFC system model, carried out the simulation, performed the post processing and analysed the data. PhD student Xiufei Li developed the MPC and PID control algorithms. Supervisors assisted in paper writing and research planning.

Paper iii: System behavior prediction by artificial neural network algorithm of a methanol steam reformer for polymer electrolyte fuel cell stack use

Y.X. Qi, J.Y. Wang, L. Wang, M. Andersson
Fuel Cells, (21)2021: 279-289

This paper proposes a novel hydrogen selective membrane reactor for MSR to produce fuel cell grade hydrogen for a PEFC system. The BP neural network algorithm is used to build the mapping model between the membrane reactor's operating parameters and PEFC system output performance. This model can be used for practical operating guidance and control applications.

The candidate organized the paper's methodology, developed the hydrogen selective membrane reactor model, proposed and validated the PEFC system model, and designed the BP algorithm. Critical guidance was received from Dr. Jingyu Wang and Docent Lei Wang. Supervisors assisted in paper writing and research planning.

Paper iv: Polymer Electrolyte Fuel Cell System Level Modelling and Simulation of Transient Behaviour

Y.X. Qi, M. Espinoza-Andaluz, M. Thern, M. Andersson
eTransportation, 2(2019): 100030

This paper reports a system level model for a polymer electrolyte fuel cell (PEFC) system, which is capable of characterizing transient behavior using the control volume method. The model was modified to test the PEFC system's application for start-up, power step-up, and shut-down response with the simulation results that show good agreement with experimental data.

The candidate organized the paper's methodology, developed the PEFC system model, and analysed the system performance. Supervisors assisted in paper writing and research planning.

References

[1] Karl Kordesch and Günter Simader. “Fuel cells and their applications”. In: (1996).

[2] Mohammad Ali Abdelkareem et al. “Environmental aspects of fuel cells: A review”. In: *Science of The Total Environment* 752 (2021), p. 141803.

[3] Xianguo Li. *Principles of fuel cells*. CRC Press, 2005.

[4] Yun Wang et al. “A review of polymer electrolyte membrane fuel cells: Technology, applications, and needs on fundamental research”. In: *Applied energy* 88.4 (2011), pp. 981–1007.

[5] Frano Barbir. *PEM fuel cells: theory and practice*. Academic press, 2012.

[6] Yanlin Ge, Lingen Chen, and Fengrui Sun. “Progress in finite time thermodynamic studies for internal combustion engine cycles”. In: *Entropy* 18.4 (2016), p. 139.

[7] “PEMFC (Proton Exchange Membrane Fuel Cells) - Global Market Trajectory Analytics”. In: (2020).

[8] M Moein-Jahromi and MJ Kermani. “Three-dimensional multiphase simulation and multi-objective optimization of PEM fuel cells degradation under automotive cyclic loads”. In: *Energy Conversion and Management* 231 (2021), p. 113837.

[9] Michael B Burkholder. “Nonlinear analysis, control, and modeling of the two-phase flow dynamics in polymer electrolyte fuel cells”. PhD thesis. Carnegie Mellon University, 2015.

[10] Michael Burkholder and Shawn Litster. “Nonlinear Diffusion Analysis of the Voltage Signal of a Polymer Electrolyte Fuel Cell with Cathode Water Accumulation”. In: *ECS Transactions* 58.1 (2013), p. 109.

[11] Mayken Espinoza Andaluz. “On Diffusion Transport Properties in Fuel Cell Gas Diffusion Layers Using the Lattice Boltzmann Method”. PhD thesis. Lund University, 2017.

[12] Kyle N Grew and Wilson KS Chiu. “A review of modeling and simulation techniques across the length scales for the solid oxide fuel cell”. In: *Journal of Power Sources* 199 (2012), pp. 1–13.

[13] Martin Andersson et al. “A review of cell-scale multiphase flow modeling, including water management, in polymer electrolyte fuel cells”. In: *Applied Energy* 180 (2016), pp. 757–778.

[14] Ambrož Kregar et al. “Predictive system-level modeling framework for transient operation and cathode platinum degradation of high temperature proton exchange membrane fuel cells”. In: *Applied Energy* 263 (2020), p. 114547.

[15] Jonas Eborn et al. “System level dynamic modeling of fuel cell power plants”. In: *Proceedings of the 2003 American Control Conference, 2003.* Vol. 3. IEEE. 2003, pp. 2024–2029.

[16] X Xue et al. “System level lumped-parameter dynamic modeling of PEM fuel cell”. In: *Journal of Power Sources* 133.2 (2004), pp. 188–204.

[17] Thomas Jahnke et al. “Performance and degradation of Proton Exchange Membrane Fuel Cells: State of the art in modeling from atomistic to system scale”. In: *Journal of Power Sources* 304 (2016), pp. 207–233.

[18] Yuyao Shan and Song-Yul Choe. “Modeling and simulation of a PEM fuel cell stack considering temperature effects”. In: *Journal of Power Sources* 158.1 (2006), pp. 274–286.

[19] Congyan Chen et al. “The Research on Anti-Interference Techniques in AMS-C Power System”. In: *Nuclear Physics B-Proceedings Supplements* 166 (2007), pp. 249–251.

[20] Jay T Pukrushpan, Anna G Stefanopoulou, and Huei Peng. *Control of fuel cell power systems: principles, modeling, analysis and feedback design.* Springer Science & Business Media, 2004.

[21] Woon Ki Na and Bei Gou. “Feedback-linearization-based nonlinear control for PEM fuel cells”. In: *IEEE Transactions on Energy Conversion* 23.1 (2008), pp. 179–190.

[22] Cristian Kunusch, Paul Puleston, and Miguel Mayosky. *Sliding-Mode control of PEM fuel cells.* Springer Science & Business Media, 2012.

[23] Carlos Andrés Ramos-Paja et al. “Minimum fuel consumption strategy for PEM fuel cells”. In: *IEEE transactions on industrial electronics* 56.3 (2008), pp. 685–696.

[24] Paulo EM Almeida and M Godoy Simoes. "Neural optimal control of PEM-fuel cells with parametric CMAC networks". In: *38th IAS Annual Meeting on Conference Record of the Industry Applications Conference, 2003.* Vol. 2. IEEE. 2003, pp. 723–730.

[25] Ali Niknezhadi et al. "Design and implementation of LQR/LQG strategies for oxygen stoichiometry control in PEM fuel cells based systems". In: *Journal of Power Sources* 196.9 (2011), pp. 4277–4282.

[26] Winston Garcia-Gabin, Fernando Dorado, and Carlos Bordons. "Real-time implementation of a sliding mode controller for air supply on a PEM fuel cell". In: *Journal of process control* 20.3 (2010), pp. 325–336.

[27] WRW Daud et al. "PEM fuel cell system control: A review". In: *Renewable Energy* 113 (2017), pp. 620–638.

[28] Vojtech Vesely and Danica Rosinová. "Robust MPC controller design for switched systems using multi-parameter dependent Lyapunov function". In: *International Journal of Innovative Computing, Information and Control* 10.1 (2014), pp. 269–280.

[29] Antonio Ferramosca et al. "Economic MPC for a changing economic criterion". In: *49th IEEE Conference on Decision and Control (CDC).* IEEE. 2010, pp. 6131–6136.

[30] Stefano Di Cairano and Alberto Bemporad. "Model predictive control tuning by controller matching". In: *IEEE Transactions on Automatic Control* 55.1 (2009), pp. 185–190.

[31] Ya-Xiong Wang and Young-Bae Kim. "Real-time control for air excess ratio of a PEM fuel cell system". In: *IEEE/ASME Transactions on Mechatronics* 19.3 (2013), pp. 852–861.

[32] Yuanxin Qi et al. "Temperature control strategy for polymer electrolyte fuel cells". In: *International Journal of Energy Research* 44.6 (2020), pp. 4352–4365.

[33] Michael A Danzer, Simon J Wittmann, and Eberhard P Hofer. "Prevention of fuel cell starvation by model predictive control of pressure, excess ratio, and current". In: *Journal of Power Sources* 190.1 (2009), pp. 86–91.

[34] C Panos et al. "Modelling and explicit model predictive control for PEM fuel cell systems". In: *Chemical Engineering Science* 67.1 (2012), pp. 15–25.

[35] CJ Jiang et al. "Kinetic study of steam reforming of methanol over copper-based catalysts". In: *Applied Catalysis A: General* 93.2 (1993), pp. 245–255.

[36] Sandra Sá et al. "Catalysts for methanol steam reforming—A review". In: *Applied Catalysis B: Environmental* 99.1-2 (2010), pp. 43–57.

[37] Binlin Dou et al. “Activity of Ni–Cu–Al based catalyst for renewable hydrogen production from steam reforming of glycerol”. In: *Energy conversion and management* 78 (2014), pp. 253–259.

[38] J Remón et al. “Production of gaseous and liquid chemicals by aqueous phase reforming of crude glycerol: influence of operating conditions on the process”. In: *Energy Conversion and Management* 110 (2016), pp. 90–112.

[39] Yaser Khojasteh Salkuyeh and Thomas A Adams II. “A new power, methanol, and DME polygeneration process using integrated chemical looping systems”. In: *Energy conversion and management* 88 (2014), pp. 411–425.

[40] Simone P Souza and Joaquim EA Seabra. “Integrated production of sugarcane ethanol and soybean biodiesel: environmental and economic implications of fossil diesel displacement”. In: *Energy conversion and management* 87 (2014), pp. 1170–1179.

[41] Noureddine Hajjaji. “Thermodynamic investigation and environment impact assessment of hydrogen production from steam reforming of poultry tallow”. In: *Energy conversion and management* 79 (2014), pp. 171–179.

[42] Yazhong Chen et al. “Hydrogen production capacity of membrane reformer for methane steam reforming near practical working conditions”. In: *Journal of Membrane Science* 322.2 (2008), pp. 453–459.

[43] George A Olah. “Beyond oil and gas: the methanol economy”. In: *Angewandte Chemie International Edition* 44.18 (2005), pp. 2636–2639.

[44] George Avgouropoulos, Alexandra Paxinou, and Stylianos Neophytides. “In situ hydrogen utilization in an internal reforming methanol fuel cell”. In: *International journal of hydrogen energy* 39.31 (2014), pp. 18103–18108.

[45] Reza Shokrani et al. “Fuel cell grade hydrogen production via methanol steam reforming over CuO/ZnO/Al2O3 nanocatalyst with various oxide ratios synthesized via urea-nitrates combustion method”. In: *International journal of hydrogen energy* 39.25 (2014), pp. 13141–13155.

[46] Yongtaek Choi and Harvey G Stenger. “Kinetics, simulation and optimization of methanol steam reformer for fuel cell applications”. In: *Journal of Power Sources* 142.1-2 (2005), pp. 81–91.

[47] Michael P Harold, Balamurali Nair, and Gregor Kolios. “Hydrogen generation in a Pd membrane fuel processor: assessment of methanol-based reaction systems”. In: *Chemical Engineering Science* 58.12 (2003), pp. 2551–2571.

[48] JR Hufton, S Mayorga, and S Sircar. “Sorption-enhanced reaction process for hydrogen production”. In: *AIChE Journal* 45.2 (1999), pp. 248–256.

[49] Marcello De Falco. “Ethanol membrane reformer and PEMFC system for automotive application”. In: *Fuel* 90.2 (2011), pp. 739–747.

[50] Dennis D Papadias et al. “An analytical and experimental investigation of high-pressure catalytic steam reforming of ethanol in a hydrogen selective membrane reactor”. In: *International journal of hydrogen energy* 35.5 (2010), pp. 2004–2017.

[51] Angelo Basile, Fausto Gallucci, and Luca Paturzo. “A dense Pd/Ag membrane reactor for methanol steam reforming: experimental study”. In: *Catalysis today* 104.2-4 (2005), pp. 244–250.

[52] Muriel Gevrey, Ioannis Dimopoulos, and Sovan Lek. “Review and comparison of methods to study the contribution of variables in artificial neural network models”. In: *Ecological modelling* 160.3 (2003), pp. 249–264.

[53] Yang Changwei et al. “Application of BP neural network model in risk evaluation of railway construction”. In: *Complexity* 2019 (2019).

[54] Marcos V Moreira and Gisele E Da Silva. “A practical model for evaluating the performance of proton exchange membrane fuel cells”. In: *Renewable Energy* 34.7 (2009), pp. 1734–1741.

[55] Jinfeng Wu et al. “Diagnostic tools in PEM fuel cell research: Part I Electrochemical techniques”. In: *International journal of hydrogen energy* 33.6 (2008), pp. 1735–1746.

[56] VB Oliveira et al. “A comparative study of approaches to direct methanol fuel cells modelling”. In: *International Journal of Hydrogen Energy* 32.3 (2007), pp. 415–424.

[57] Attia A El-Fergany. “Extracting optimal parameters of PEM fuel cells using Salp Swarm Optimizer”. In: *Renewable Energy* 119 (2018), pp. 641–648.

[58] M Kandidayeni et al. “Benchmark of proton exchange membrane fuel cell parameters extraction with metaheuristic optimization algorithms”. In: *Energy* 183 (2019), pp. 912–925.

[59] Ronald F Mann et al. “Development and application of a generalised steady-state electrochemical model for a PEM fuel cell”. In: *Journal of power sources* 86.1-2 (2000), pp. 173–180.

[60] Majid Ali, MA El-Hameed, and MA Farahat. “Effective parameters’ identification for polymer electrolyte membrane fuel cell models using grey wolf optimizer”. In: *Renewable energy* 111 (2017), pp. 455–462.

[61] PR Pathapati, X Xue, and J Tang. “A new dynamic model for predicting transient phenomena in a PEM fuel cell system”. In: *Renewable energy* 30.1 (2005), pp. 1–22.

[62] James Larminie, Andrew Dicks, and Maurice S McDonald. *Fuel cell systems explained*. Vol. 2. J. Wiley Chichester, UK, 2003.

[63] Jeferson M Corrêa et al. "An electrochemical-based fuel-cell model suitable for electrical engineering automation approach". In: *IEEE Transactions on industrial electronics* 51.5 (2004), pp. 1103–1112.

[64] MJ Khan and MT Iqbal. "Modelling and analysis of electro-chemical, thermal, and reactant flow dynamics for a PEM fuel cell system". In: *Fuel cells* 5.4 (2005), pp. 463–475.

[65] K Sankar, Koushik Aguan, and Amiya K Jana. "A proton exchange membrane fuel cell with an airflow cooling system: Dynamics, validation and nonlinear control". In: *Energy Conversion and Management* 183 (2019), pp. 230–240.

[66] Jay T Pukrushpan, Huei Peng, and Anna G Stefanopoulou. "Simulation and analysis of transient fuel cell system performance based on a dynamic reactant flow model". In: *ASME International Mechanical Engineering Congress and Exposition*. Vol. 36290. 2002, pp. 637–648.

[67] Abdul Afram and Farrokh Janabi-Sharifi. "Theory and applications of HVAC control systems–A review of model predictive control (MPC)". In: *Building and Environment* 72 (2014), pp. 343–355.

[68] Štefan Kozák. "From PID to MPC: Control engineering methods development and applications". In: *2016 Cybernetics & Informatics (K&I)*. IEEE. 2016, pp. 1–7.

[69] Chen Chen et al. "MPC-based appliance scheduling for residential building energy management controller". In: *IEEE Transactions on Smart Grid* 4.3 (2013), pp. 1401–1410.

[70] Marek Honek et al. "A low-complexity explicit MPC controller for AFR control". In: *Control Engineering Practice* 42 (2015), pp. 118–127.

[71] Hengyang Wang et al. "Path tracking control for autonomous vehicles based on an improved MPC". In: *IEEE Access* 7 (2019), pp. 161064–161073.

[72] G Ganga and Meher Madhu Dharmana. "MPC controller for trajectory tracking control of quadcopter". In: *2017 International Conference on Circuit, Power and Computing Technologies (ICCPCT)*. IEEE. 2017, pp. 1–6.

[73] Antonio Ferramosca et al. "MPC for tracking zone regions". In: *Journal of Process Control* 20.4 (2010), pp. 506–516.

[74] GC Goodwin et al. "Applications of MPC in the Area of Health Care". In: *Handbook of Model Predictive Control*. Springer, 2019, pp. 529–550.

[75] Veronica Adetola and Martin Guay. “Robust adaptive MPC for constrained uncertain nonlinear systems”. In: *International Journal of Adaptive Control and Signal Processing* 25.2 (2011), pp. 155–167.

[76] Jung-Su Kim. “Recent advances in adaptive MPC”. In: *ICCAS 2010*. IEEE. 2010, pp. 218–222.

[77] Monimoy Bujarbaruah, Xiaojing Zhang, and Francesco Borrelli. “Adaptive MPC with chance constraints for FIR systems”. In: *2018 Annual American Control Conference (ACC)*. IEEE. 2018, pp. 2312–2317.

[78] Merit Bodner et al. “Enabling industrial production of electrodes by use of slot-die coating for HT-PEM fuel cells”. In: *International Journal of Hydrogen Energy* 44.25 (2019), pp. 12793–12801.

[79] Y-L Ma et al. “Conductivity of PBI membranes for high-temperature polymer electrolyte fuel cells”. In: *Journal of the Electrochemical Society* 151.1 (2003), A8.

[80] MR Islam et al. “The potential of using nanofluids in PEM fuel cell cooling systems: A review”. In: *Renewable and Sustainable Energy Reviews* 48 (2015), pp. 523–539.

[81] Yuki Kitami, Yutaka Tabe, and Takemi Chikahisa. “Control of the Balance between Vapor and Heat Transfer for the Reduction of Oxygen Transport Resistance in High Current Density PEFC Operation”. In: *ECS Transactions* 92.8 (2019), p. 213.

[82] Fu-Cheng Wang et al. “Multivariable robust control of a proton exchange membrane fuel cell system”. In: *Journal of Power Sources* 177.2 (2008), pp. 393–403.

[83] Pang-Chia Chen. “The dynamics analysis and controller design for the PEM fuel cell under gas flowrate constraints”. In: *International Journal of Hydrogen Energy* 36.4 (2011), pp. 3110–3122.

[84] Xinhai Xu, Kaipeng Shuai, and Ben Xu. “Review on copper and palladium based catalysts for methanol steam reforming to produce hydrogen”. In: *Catalysts* 7.6 (2017), p. 183.

[85] Patrick Kurr et al. “Microstructural characterization of Cu/ZnO/Al2O3 catalysts for methanol steam reforming—A comparative study”. In: *Applied Catalysis A: General* 348.2 (2008), pp. 153–164.

[86] Brant A Peppley et al. “Methanol–steam reforming on Cu/ZnO/Al2O3. Part 1: the reaction network”. In: *Applied Catalysis A: General* 179.1-2 (1999), pp. 21–29.

[87] Yuting Zhang et al. “Hydrogen-selective zeolite membrane reactor for low temperature water gas shift reaction”. In: *Chemical engineering journal* 197 (2012), pp. 314–321.

[88] Nisha Katiyar, Shashi Kumar, and Surendra Kumar. “Polymer electrolyte membrane fuel cell grade hydrogen production by methanol steam reforming: a comparative multiple reactor modeling study”. In: *Journal of power sources* 243 (2013), pp. 381–391.

[89] NA Al-Mufachi, NV Rees, and R Steinberger-Wilkens. “Hydrogen selective membranes: A review of palladium-based dense metal membranes”. In: *Renewable and Sustainable Energy Reviews* 47 (2015), pp. 540–551.

[90] Shifei Ding, Chunyang Su, and Junzhao Yu. “An optimizing BP neural network algorithm based on genetic algorithm”. In: *Artificial intelligence review* 36.2 (2011), pp. 153–162.

[91] Rajesh Kumar, RK Aggarwal, and JD Sharma. “Energy analysis of a building using artificial neural network: A review”. In: *Energy and Buildings* 65 (2013), pp. 352–358.

[92] SM Sharifi Asl, S Rowshanzamir, and MH Eikani. “Modelling and simulation of the steady-state and dynamic behaviour of a PEM fuel cell”. In: *Energy* 35.4 (2010), pp. 1633–1646.

[93] John C Amphlett et al. “A model predicting transient responses of proton exchange membrane fuel cells”. In: *Journal of Power sources* 61.1-2 (1996), pp. 183–188.

[94] AA Abd El Monem, Ahmed M Azmy, and SA Mahmoud. “Effect of process parameters on the dynamic behavior of polymer electrolyte membrane fuel cells for electric vehicle applications”. In: *Ain Shams Engineering Journal* 5.1 (2014), pp. 75–84.

[95] Mohsen Kandidayeni et al. “Optimized Fuzzy Thermal Management of an Open Cathode Fuel Cell System”. In: *2018 IEEE Vehicle Power and Propulsion Conference (VPPC)*. IEEE. 2018, pp. 1–6.

[96] Fabio Musio et al. “PEMFC system simulation in MATLAB-Simulink® environment”. In: *International Journal of Hydrogen Energy* 36.13 (2011), pp. 8045–8052.

[97] F Gallucci et al. “The effect of the hydrogen flux pressure and temperature dependence factors on the membrane reactor performances”. In: *International journal of hydrogen energy* 32.16 (2007), pp. 4052–4058.